POL2000
July 15, 2003

A New Analysis for the Transverse Polarimeter at HERA II

T. Behnke, J. Böhme, B. List, S. Schmitt

Abstract

The HERA ep–collider provides a longitudinally polarised positron beam to the three experiments HERMES, H1 and ZEUS. The degree of polarisation is determined with two Compton polarimeters, one measuring the transverse polarisation that naturally builds up in a sufficiently planar ring via the Sokolov–Ternov effect, the other one measuring the longitudinal polarisation between the HERMES spin rotators. The future physics program of the collider experiments requires polarimetry with a precision of better than 1%. To meet this goal, the Transverse Polarimeter has been upgraded in 2001 with a new data acquisition system and a silicon strip detector complementing the main calorimeter. A new analysis, which allows an in–situ calibration in paralel to the polarisation measurement without relying on testbeam results obtained under different conditions, is presented in this paper. The new method uses a fit of the double–differential Compton cross section (folded with detector effects) to the measured two–dimensional spectra in energy and position of the scattered photon. In March 2003, HERA succeeded to deliver up to 50% of longitudinal polarisation to all three experiments as well as collisions for H1 and ZEUS. Some first results of the new analysis on polarised HERA II data are shown.

1 Introduction

In the HERA storage ring at DESY, Hamburg, which is shown in figure 1, electrons (or positrons) with an energy of 27.5 GeV collide with 920 GeV protons in two interaction regions, where the experiments H1 and ZEUS are installed. Furthermore two fixed target experiments, HERMES and HERA–B, make use of only the electron or proton beam, respectively. The electron beam at HERA can be tuned such that it becomes transversely polarised via the Sokolov–Ternov effect [1]. At HERA I (until the year 2000), only the HERMES interaction region was surrounded by special chains of magnets rotating the spin of the electrons in order to achieve longitudinal polarisation. After HERA had been upgraded for higher luminosity in 2001 (HERA II), additional spin rotators were installed at H1 and ZEUS. The future physics program of the two collider experiments requires polarimetry with a precision of 1% or better, which has never been reached before at HERA.

The degree of polarisation is measured by two polarimeters, both making use of the polarisation dependency of Compton scattering. The Transverse Polarimeter (TPOL) is located near the HERA–B interaction region where the polarisation vector is oriented vertically, and the Longitudinal Polarimeter (LPOL) measures between the HERMES spin rotators, where the polarisation vector is oriented along the beam axis. While the LPOL remained more or less unchanged awaiting a later upgrade, the TPOL has been improved substantially during the luminosity upgrade in order to deliver a polarisation measurement of increased precision not only to HERMES, but also to the H1 and ZEUS experiments.

Although discussed in detail later, the principle of measurement shall be explained briefly here. While longitudinal polarisation of the lepton beam influences the energy spectrum of the backscattered photons, transverse polarisation causes an energy dependent asymmetry of the scattering rate with respect to the direction of the polarisation vector. Thus, the TPOL needs to measure the vertical position of each single scattered photon. The main detector is a calorimeter which is segmented in an upper and lower half, giving the photon's energy as the sum of both channels, while the energy asymmetry between upper and lower half is a measure for the vertical position. The exact relationship between position and energy asymmetry (also called "η–y–transformation"), which depends delicately on the transverse shower development in the calorimeter, is a priori unknown and used to be the dominant source of systematic uncertainty.

During the actual measurement, the number of detected photons is accumulated in bins of position and energy over a time period giving a sufficiently small statistical uncertainty. From such a two–dimensional spectrum the up–down asymmetry and thus the degree of vertical polarisation is extracted.

This paper presents the progress made in terms of detector understanding and analysis technique in order to meet the new precision requirements with the TPOL.

2 The Transverse Polarimeter

The TPOL has been in operation since 1992. Although its basic properties have already been described in [2], a brief overview will be given here, including the recent changes to the polarimeter. The general setup is shown in figure 2. The light of a continuous wave laser with a wavelength of 514.5 nm ($E_\lambda = 2.41$ eV) and a power of 10 W is guided into the HERA tunnel with various mirrors, some of them adjustable, and focussed onto the circulating electron beam under a crossing angle of 3.1 mrad. The laser power is chosen such that the probability for a Compton interaction per bunch is about 1/1000. Since the spacing of the 220 bunches in the ring is 96 ns, this leads to an interaction rate of about 10 kHz with a negligible probability for an overlay of two (or even more) simultaneous scattering processes. The laser beam is circularly polarised to up to 99.5% by a Pockel's cell. The backscattered Compton photons are detected 65 m downstream, where the dipoles of the next arc section bend the electron beam away from the photons. The main part of the detector is a Tungsten–Scintillator–sampling calorimeter, which has already been described in [2]. During the upgrade it has been replaced by an identical spare calorimeter. The detector has been complemented by a silicon strip detector in front of the calorimeter, which is intended to calibrate the position measurement by the calorimeter directly during the polarisation measurement. This required two additional new components shown in figure 3: a preradiator of one radiation length of lead is placed a few centimeters in front of the detector in order to increase the interaction probability in the silicon, and a movable scintillating fiber which has been installed just in front of the silicon for monitoring the performance of the silicon detector with respect to possible radiation damage.

A central issue of the upgrade is a new data acquisition system for the TPOL, which now is capable to accumulate and read out the two–dimensional spectra for all 220 bunches separately. This is required since the degree of polarisation is usually different for electron bunches that collide with proton bunches in the IPs and the non–collinding bunches, which are only used by HERMES but do not contribute to the luminosity of H1 and ZEUS. Further advantages of the new DAQ are a much better linearity of the FADCs, online pedestal subtraction and less noise.

The measurement proceeds as follows. For about 20 seconds, the laser beam is interrupted by a shutter, allowing to measure the background which is dominated by bremsstrahlung. For the next 40 seconds, the shutter is opened and the laser polarisation is switched between the left handed and right handed state with a frequency of 90 Hz. Two-dimensional histograms in the photon's total energy E and energy asymmetry η are accumulated separately for the "laser left", "laser right" and "laser off" states. A fast online analysis using the analysing power technique described briefly in section 4 then calculates the current polarisation value, which is distributed to the machine control room as well as to the three experiments. For several reasons, this online measurement is not able to achieve the precision required by the physics program of the collider experiments. Therefore a new offline analysis has been developed, which will be presented in the section 5.

3 Compton Scattering as Measurement Principle

Figure 4 shows schematically a Compton Scattering process in the electron restframe and in the laboratory frame. k_i and k_f denote the momentum of the incoming and outgoing photon in the electron restframe, respectively:

$$k_\mathrm{i} = 2\gamma E_\lambda / m_\mathrm{e} = 2 E_\mathrm{e} E_\lambda / {m_\mathrm{e}}^2 \tag{1}$$

$$k_\mathrm{f} = 1/(1 - \cos\theta + 1/k_\mathrm{i}) \tag{2}$$

Here γ denotes the Lorentz boost of the laboratory frame with respect to the electron rest frame, E_λ the energy of the laser photons, m_e the electron rest mass and θ the scattering angle in the restframe as indicated in figure 4. At HERA, $k_\mathrm{i} = 0.508$. The angle θ is uniquely determined by the photon energy E in the laboratory frame — therefore, photons of the same energy form concentric circles on the detector surface:

$$\cos\theta = \frac{E_\mathrm{e} - E(1 + 1/k_\mathrm{i})}{E_\mathrm{e} - E} \tag{3}$$

The most energetic photons are located in the center at $\theta = 180°$, and their energy is given by:

$$E_\mathrm{max} = \frac{2E_\mathrm{e}}{2 + 1/k_\mathrm{i}} \tag{4}$$

The radius of a circle for a fixed photon energy is

$$R(E) = D\tan\theta_\mathrm{lab} = \frac{D}{\gamma\tan\theta/2} \tag{5}$$

where D is the distance between the detector and the laser–electron interaction point. The azimutal angle ϕ is connected to the vertical coordinate on the detector surface if its energy is known[1]:

$$y = R\,(E)\,\sin\phi \tag{6}$$

The double differential cross section of Compton scattering can be devided into several terms according to their polarisation dependence:

$$\frac{d^2\sigma}{\mathrm{d}E\,d\phi} = \Sigma_0(E) + S_1\Sigma_1(E)\cos 2\phi + S_3(P_\mathrm{Y}\Sigma_{2\mathrm{Y}}(E)\sin\phi + P_\mathrm{Z}\Sigma_{2\mathrm{Z}}(E)) \tag{7}$$

Here, S_1 and S_3 denote the linear and circular laser polarisations and P_Y and P_Z the transverse and longitudinal components of the electron beam polarisation. The Σ functions depend only on the scattered photon's energy, the angular dependecies are given explicitly. From the above formula, the measurement principles for TPOL and LPOL can be seen easily. After integration over ϕ, the term depending on the transverse polarisation vanishes, while the term proportional to P_Z remains. For the LPOL it is thus sufficient to measure the energy spectrum of the scattered photons, whereas the TPOL needs to measure both their energy and their position in order to extract P_Y. Since flipping the helicity of the laser means changing the sign of S_3, the dependence on the beam polarisations will drop out when adding the spectra for left and right handed laser states, providing an ideal tool for calibration purposes independent of the beam polarisation:

$$\frac{d^2\sigma}{\mathrm{d}E\,\mathrm{d}\phi}(R + L) = 2\Sigma_0(E) + 2S_1\Sigma_1(E)\cos 2\phi \tag{8}$$

Assuming S_1 remains unchanged by the helicity flip, the difference of the spectra for the same two states leaves us only with the beam polarisation dependent terms:

$$\frac{d^2\sigma}{\mathrm{d}E\,\mathrm{d}\phi}(R - L) = 2S_3(P_\mathrm{Y}\Sigma_{2\mathrm{Y}}(E)\sin\phi + P_\mathrm{Z}\Sigma_{2\mathrm{Z}}(E)) \tag{9}$$

[1]The left–right ambiguity doesn't need to be resolved here, since the vertical beam polarisation is of interest, whereas any possible horizontal component can safely be neglected.

In reality one has to take into account that the flipping of the laser helicity also changes S_1 and the size of S_3 (and not only its sign). The laser parameters are tuned such that the additional terms are as small as possible, but it turns out that they can not be completely neglected for a high precision analysis:

$$\frac{\mathrm{d}^2\sigma}{\mathrm{d}E\,\mathrm{d}\phi}(R+L) = 2\Sigma_0 + (S_1^R + S_1^L)\Sigma_1 \cos 2\phi + (S_3^R + S_3^L)(P_\mathrm{Y}\Sigma_{2\mathrm{Y}} \sin\phi + P_\mathrm{Z}\Sigma_{2\mathrm{Z}}) \quad (10)$$

$$\frac{\mathrm{d}^2\sigma}{\mathrm{d}E\,\mathrm{d}\phi}(R-L) = (S_1^R - S_1^L)\Sigma_1 \cos 2\phi + (S_3^R - S_3^L)(P_\mathrm{Y}\Sigma_{2\mathrm{Y}} \sin\phi + P_\mathrm{Z}\Sigma_{2\mathrm{Z}}) \quad (11)$$

Since these two equations form the foundation of the offline analysis, which will be discussed in detail in section 5, the actual formulae for Σ_0, Σ_1, $\Sigma_{2\mathrm{Y}}$ and $\Sigma_{2\mathrm{Z}}$ will be given here, where the photon energy E has been replaced by the normalised energy $x = E/E_\mathrm{e}$:

$$\Sigma_0 = C(x)\,(-x^3 + (2 + (1 + 1/k_\mathrm{i})^2)x^2 - 4x/x_\mathrm{max} + 2) \quad (12)$$

$$\Sigma_1 = C(x)\,x^2/{k_\mathrm{i}}^2\,(2k_\mathrm{i}(1/x - 1) - 1) \quad (13)$$

$$\Sigma_{2\mathrm{Y}} = C(x)\,x^2/k_\mathrm{i}\,(x-1)\sqrt{2k_\mathrm{i}(1/x-1) - 1} \quad (14)$$

$$\Sigma_{2\mathrm{Z}} = C(x)\,((1 + 1/k_\mathrm{i})\,x - 1)\,x^2 \quad (15)$$

The common factor $C(x)$ is given by:

$$C(x) = \frac{r_0^2}{2k_\mathrm{i}E_\mathrm{e}(1-x)^2} \quad (16)$$

where $r_0 = 2.818\,\mathrm{fm}$ is the classical electron radius.

4 The Average η Method with Constant Analysing Power

The average η method, which is used for the online polarisation measurement, shall be briefly explained here for later comparisions. It been described in detail in [2].

For each of the laser helicity states, the average η value in a certain energy slice is calculated from the two–dimensional spectra collected when the laser is on and corrected for the background contribution with the help of the corresponding spectra taken when the laser is shut off. The difference of these mean η values depends on the beam polarisation, because the up–down asymmetry in the scattering rate grows with the degree of polarisation. The relation is assumed to be linear and the proportionality constant Π, called analysing power, is the difference that is expected for 100% polarisation:

$$P_\mathrm{Y} = \Pi\,\frac{\bar{\eta}_R - \bar{\eta}_L}{2} \quad (17)$$

The analysing power can be estimated from Monte Carlo simulations and calibrated with risetime measurements [2], but it is assumed to be constant with respect to all system parameters like resolutions, η–y–transformation, beam position and spot size or the residual linear laser polarisation. This assumption finally limits the precision of this method. Some of the system parameters, namely table position, beam spot size, the difference of the linear polarisation components of the two laser helicity states and the relative miscalibration of the calorimeter channels are also extracted, but used only to control the hardware.

5 The Offline Analysis

This section describes the full analysis of the TPOL data as it has been developed for a high precision polarisation measurement. For each one–minute measurement cycle the Compton signal is extracted by subtracting the bremsstrahlung background[2] measured when the laser is shut off. After that, the Compton edge in the energy spectrum is used for an absolute energy calibration of the calorimeter. These two steps are described in section 5.1. Once the energy scale has been calibrated, the full two–dimesional spectra of η vs E taken with right and left handed circular laser polarisation are fitted by the double–differential cross section for Compton scattering folded with the parametrised effects of the system parameters. This fit is discussed in detail in section 5.3. It uses a parametrisation of the energy and position resolution of the calorimeter obtained from GEANT simulation studies presented in section 5.2. In section 5.4 the new analysis is applied to data taken in March 2003, when a polarisation of up to 50% was achieved. During this period the general conditions were rather instable, limiting the conclusion that can be drawn from these first measurements. Tests of the fit performance based on a fast parametrised Monte Carlo simulation are discussed in section 5.5.

5.1 Background Subtraction and Energy Calibration

In the first step of the analysis, the background, which is measured separately when the laser is shut off, is subtracted. An example of a laser "ON", laser "OFF" and a background subtracted energy spectrum is shown in figure 5. The energy calibration of the calorimeter is performed on the resulting background subtracted energy spectrum which shows the prominent Compton edge. The whole spectrum can be well described by the compton cross section, folded with the energy resolution of the calorimeter and cut off at low energies by a trigger threshold parametrised as Fermi function. Fitting the number of ADC counts per GeV (parameter 2 in figure 5), the energy resolution (parameter 3), position and width of the trigger threshold (parameters 4 and 5), the overall normalisation (parameter 1) and the remaining background fraction (parameter 6), the position of the Compton edge, which is used for energy calibration, can be determined with a precision of half a permille per minute.

5.2 Energy and Position Resolution

The energy and position resolution of the calorimeter has been studied using a GEANT [6] simulation, in order to arrive at a consistent description of both resolutions from the energy measurements in the two halfs of the calorimeter and their covariance matrix.

Let us consider first the energy resolution. If one adds the energies E_u and E_d measured in both halves of the calorimeter to get the full photon energy $E = E_\mathrm{u} + E_\mathrm{d}$, the energy resolution should not depend on the impact position y and it should be possible to parametrised it as

$$\sigma_E^2 = a^2 E + b^2 E^2 \tag{18}$$

Monte Carlo studies show that the parameters a and b indeed do not depend on y, as shown in Fig. 6.

[2]There are also other background contributions. For a detailed discussion see [5]

If one uses a similar ansatz for the individual measurements of E_u and E_d, i. e. $\sigma^2_{Eu} = a_u^2 E_\mathrm{u} + b_u^2 {E_\mathrm{u}}^2$, one finds that the coefficients a_u and b_u do depend on y.

However, the demand that Eq. (18) should describe the resolution of the sum $E = E_\mathrm{u} + E_\mathrm{d}$ leads to the ansatz

$$C_{\mathrm{u,d}} = \begin{pmatrix} a^2 E_\mathrm{u} + b^2 {E_\mathrm{u}}^2 + s^2(E,\eta) & -s^2(E,\eta) + b^2 E_\mathrm{u} E_\mathrm{d} \\ -s^2(E,\eta) + b^2 E_\mathrm{u} E_\mathrm{d} & a^2 E_\mathrm{d} + b^2 {E_\mathrm{d}}^2 + s^2(E,\eta) \end{pmatrix}, \tag{19}$$

for the covariance matrix between E_u and E_d. This covariance matrix treats the halves of the calorimeter as two independent calorimeters with the same energy resolution as that of the overall calorimeter if η is close to ± 1, i. e. the energy is deposited in one half alone. The term $s^2(E,\eta)$ describes the degradation of the resolution due to "leakage" into the other half. The amount of energy that "leaks out" is anticorrelated between the two halves and therefore does not affect the overall energy resolution.

The position resolution or, more precisely, the resolution of the energy asymmetry $\eta = (E_\mathrm{u} - E_\mathrm{d})/(E_\mathrm{u} + E_\mathrm{d})$ can now be derived from this covariance matrix by straight–forward error propagation:

$$\sigma^2_\eta = \frac{(1-\eta^2)a^2}{E} + \frac{4s^2(E,\eta)}{E^2} \tag{20}$$

The first term in the equation above has already been taken into account in previous analyses [2], where as the second term refines the parametrisation, leading to a better description of the data. The energy and η dependence of s^2 has been investigated with the GEANT simulation. It is found to be reasonably well described by the form

$$\frac{s^2(E,\eta)}{E^2} = f^2(\eta)\frac{\sqrt{1-\eta^2}}{E} + g^2(\eta)(1-\eta^2) \tag{21}$$

where $f^2(\eta)$ represents the sum of two Gaussians and $g^2(\eta)$ a Gaussians added to a constant function as shown in Fig.7. With the final set of parameters taken from GEANT they are:

$$\begin{aligned} f^2(\eta) &= 0.018 \cdot \exp\frac{-\eta^2}{2\cdot 0.14^2} + 0.057 \cdot \exp\frac{-\eta^2}{2\cdot 0.45^2} & (22) \\ g^2(\eta) &= 0.00022 \cdot \exp\frac{-\eta^2}{2\cdot 0.088^2} + 0.0012 & (23) \\ & & (24) \end{aligned}$$

The parameter a is fitted from the data, while the value of b is taken from the GEANT simulation. It has also been tried to scale the size of the s^2/E^2 term in the fit, but the minimal χ^2 was reached for a scale factor equal to unity within errors, allowing the conclusion that the parametrisation of the GEANT results is sufficient to describe the data.

5.3 The Fitting Procedure

The main ingredient of the TPOL offline analysis is a fit of a two–dimensional function to the background–subtracted data, binned in E and η. The fit function is based on the Compton scattering cross section, and includes the effects caused by the beam size, the non–ideal polarisation of the laser, and detector effects, i. e. the energy resolution and η–y–transformation of the calorimeter. Altogether 10 parameters are needed to describe these effects, and several more have been investigated.

The exact construction of the fit function and the meaning of its parameters is discussed in the following subsections. In a first fit, the data spectra taken with left and right handed circular laser polarisation are added, so that the term dependent on the beam polarisation vanishes. This allows to determine all other system parameters independent from the quantity to be measured in the end, i. e. the beam polarisation. After that, all parameters from the first fit are fixed, especially the overall normalisation, and the difference of the data spectra taken with the two laser polarisation states is fitted with only the beam polarisation and the difference of the linear laser polarisation components as free parameters. These two fitting stages, also called “calibration fit” and “polarisation fit” are described in subsections 5.3.4 and 5.3.5

5.3.1 The Fit Function

The function to be fitted to the measured two–dimensional spectra is constructed in several steps:

1. The parts Σ_0, Σ_1 and Σ_{2Y} of the double differential cross section (see equation 7) are histogrammed two–dimensionally as function of the photon's energy E and azimutal angle ϕ. The resulting histograms are added according to the linear component S_1 of the laser polarisation and the product of circular laser polarisation and beam polarisation $S_3 P_\mathrm{Y}$, which are varied by the fit.

2. Next, the ϕ axis is transformed into the y coordinate, thus making the transition from $d^2\sigma/\mathrm{d}E\,\mathrm{d}\phi$ to $d^2\sigma/\mathrm{d}Edy$. Since the derivative $\mathrm{d}\phi/\mathrm{d}y$ appearing in the transformation has singularities for certain values of y and E, a special numerical method is used which is described in the next subsection. After this transformation, the fit allows for an offset between beam axis and center of the calorimeter δy.

3. In order to take into account a finite and variable size of the electron beam, a gaussian smearing of the y coordinate is performed according to a further fit parameter representing the effective width of the beam spot σ_y.

4. Next, the η–y–transformation is applied, again using the resampling technique. It is expressed as function of five fit parameters:

   $$\eta\,(y) = \mathrm{sign}\,(y)(1 - C_1 e^{-|y|/\lambda_1} - (1 - C_1 - C_2)e^{-|y|/\lambda_2} - C_2 e^{-|y|/\lambda_3}) \qquad (25)$$

   The functional form is inspired by the integral of the transverse shower shape, which is assumed to consist of three exponential parts falling off differently fast with increasing distance from the shower centre. It has also been tried to use only two exponential terms, but this leads to a significantly worse description of the data.

5. Finally, the calorimeter response, parametrised as described in section 5.2, is taken into account by applying a two dimensional gaussian smearing in E and η. This includes also the effect of a different energy response of the two halves of the calorimeter as described in section 5.3.3

The histogram obtained after step 5 is then compared to the data. A χ^2 is calculated by adding up the squares of the binwise differences divided by the statistical error of the data. This χ^2 is then minimised by the MINUIT [4] package as a function of above parameters. All bins between 5.8 GeV $< E <$ 16.4 GeV and $-0.6875 < \eta < 0.65625$ which are non–empty in the data histogram are used in the fit, resulting in approximately 2000 degrees of freedom.

5.3.2 The Resampling Method

The resampling method is used to perform a coordinate transformation of a double–differential distribution, e.g.

$$\frac{\mathrm{d}^2\sigma}{\mathrm{d}x_1\,\mathrm{d}y_1} \to \frac{\mathrm{d}^2\sigma}{\mathrm{d}x_2\,\mathrm{d}y_2},$$

where (x_2, y_2) is a function of (x_1, y_1). In our analysis, this resampling is used for example for the transformation

$$\frac{\mathrm{d}^2\sigma}{\mathrm{d}E\,\mathrm{d}\phi} \to \frac{\mathrm{d}^2\sigma}{\mathrm{d}E\,\mathrm{d}y}$$

with $y = R\,(E) \cdot \sin(\phi)$.

The analytic expression for this transition is given by

$$\frac{\mathrm{d}^2\sigma}{\mathrm{d}x_1\,\mathrm{d}y_1} \to \frac{\mathrm{d}^2\sigma}{\mathrm{d}x_2\,\mathrm{d}y_2} = \frac{\mathrm{d}^2\sigma}{\mathrm{d}x_1\,\mathrm{d}y_1} \cdot \left|\frac{\partial x_1, y_2}{\partial x_2, y_2}\right|$$

with the well-known Jacobi determinant

$$\left|\frac{\partial x_1, y_1}{\partial x_2, y_2}\right| = \frac{\partial x_1}{\partial x_2} \cdot \frac{\partial y_1}{\partial y_2} - \frac{\partial x_1}{\partial y_2} \cdot \frac{\partial y_1}{\partial x_2}.$$

In our case, this determinant is given by

$$\left|\frac{\partial E, y}{\partial E, \phi}\right| = \frac{\partial \phi}{\partial y} - \frac{\partial E}{\partial y} \cdot \frac{\partial \phi}{\partial E}. = \frac{1}{R\,(E) \cdot \cos\phi},$$

which becomes singular for $\phi = \pm\pi/2$. This singularity hampers all analytic calculations involving $\mathrm{d}^2\sigma/\mathrm{d}E\,\mathrm{d}y$ itself, and makes it numerically problematic to even fill a histogram with an accurate value of $\mathrm{d}^2\sigma/\mathrm{d}E\,\mathrm{d}y$ directly.

The resampling method (Fig. 8) now works as follows: The starting point is two–dimensional histogram with the distribution in terms of the variables (x_1, y_1). Each bin is divided into two triangles; these triangles are transformed into triangles in the (x_2, y_2) plane by applying the transformation $(x_1, y_1) \to (x_2, y_2)$ to the coordinates of the triangle's vertices. Now the tranformed triangles are intersected with the bin boundaries of the target histogram in the (x_2, y_2) plane. The area of the intersection of each triangle with a given target bin is then divided by the total area of the transformed triangles, and the bin contents of the original bin are distributed over the bins in the target histogram according to the respective area fractions. If c_i denotes the bin contents of the i-th bin in the source histogram, and C_j the contents of the j-th bin in the target histogram, one can write the resampling as

$$C_\mathrm{j} = \sum_i f_\mathrm{ij} \cdot c_\mathrm{i},$$

where f_{ij} denotes the area fraction of the transformed source bin i that falls into target bin j. For those source bins i that fall completely into the (x_2, y_2) region covered by the target histogram, the coefficients f_{ij} fulfill the condition

$$\sum_j f_{\mathrm{ij}} = 1.$$

Thus, the resampling method ensures that the overall normalisation of the cross section is unaffected by the transformation. Therefore, if the initial histogram is binned in coordinates in which the cross section varies smoothly, such as (E, ϕ) in the case of Compton scattering, the histogram in the transformed coordinates, such as (E, y), is also correctly normalised.

Since the calculation of the coefficients f_{ij} is expensive in terms of computing power, but most of the f_{ij} are 0 (typically, only 10 coefficients for fixed i are nonzero), the coefficients can be stored, and the actual resampling can be implemented as a (sparse) matrix multiplication. Thus it is possible to transform a histogram with 10000 bins or more very fast.

5.3.3 Photomultiplier Gain Difference

The resampling method is also used to describe the effect of a gain difference between the lower and upper photomultiplier. If $\eta\,(y)$ denotes the ideal η–y–transformation, then for a given photon energy E the energies E_{u} (E_{d}) that are deposited in the upper (lower) part of the calorimeter are given by

$$E_{\mathrm{u}} = \frac{1 + \eta\,(y)}{2} \cdot E, \qquad E_{\mathrm{d}} = \frac{1 - \eta\,(y)}{2} \cdot E.$$

If we now assume that the gains g_{u} (g_{d}) of the upper (lower) photomultiplier are given in terms of the mean gain g and the gain variation δg as

$$g_{\mathrm{u}} = g + \delta g, \qquad g_{\mathrm{d}} = g - \delta g,$$

then the respective photomultiplier signals S_{u} (S_{d}) are given by

$$S_{\mathrm{u}} = (g + \delta g) \cdot \frac{1 + \eta\,(y)}{2} \cdot E, \qquad S_{\mathrm{d}} = (g - \delta g) \cdot \frac{1 - \eta\,(y)}{2} \cdot E.$$

The total signal is then

$$S = S_{\mathrm{u}} + S_{\mathrm{d}} = (g + \delta g\, \eta) \cdot E.$$

Since the energy calibration procedure determines g mainly from the position of the Compton edge, which lies at $\eta = 0$, the reconstruced energy is given by

$$E_{\mathrm{rec}} = S/g = \left(1 + \frac{\delta g}{g} \eta\right) E.$$

The reconstructed value η_{rec} is given by

$$\eta_{\mathrm{rec}} = \frac{S_{\mathrm{u}} - S_{\mathrm{d}}}{S_{\mathrm{u}} + S_{\mathrm{d}}} = \frac{(g + \delta g) \cdot (1 + \eta) - (g - \delta g) \cdot (1 - \eta)}{(g + \delta g) \cdot (1 + \eta) + (g - \delta g) \cdot (1 - \eta)} \tag{26}$$

$$= \frac{\eta + \delta g/g}{1 + \eta \cdot \delta g/g} \approx \eta + (1 - \eta^2)\frac{\delta g}{g}. \tag{27}$$

The relative photomultiplier gain difference $\delta g/g$ therefore results in a energy miscalibration that depends linearly on η, and in a quadratic shift of the reconstructed η_{rec} that is maximal in the center at $\eta = 0$, where its value is $\delta\eta = \delta g/g$, and that vanishes at $\eta = \pm 1$.

It is interesting to note that the effect of such a gain difference and the effect from a imperfect centering of the calorimeter with respect to the photon beam center are sufficiently different to allow a distinction of both by the fitting procedure. Fig. 9 illustrates the reason for that: while a shift of the calorimeter in y leaves the η–y–transformation symmetric, a change of the relative photomultiplier gains leads to a visibly asymmetric form of the transformation.

5.3.4 The Calibration Fit

The calibration fit can be performed in different modi, depending on the number of parameters that are fixed. In the full mode, the fit is allowed to vary all system parameters including those which are expected to change only slowly with time like the η–y–transformation or the energy resolution. The full set of fit parameters comprises:

- σ_y: transverse gaussian width of the Compton interaction region, also referred to as beam spot size, which is determined to the accelerator optics and emittance as well as on the distance between Compton interaction point and calorimeter. Typical values are in the order of 0.5 mm.

- δ_y: vertical offset between positron beam axis and center of the calorimeter. The online analysis monitors this offset and corrects for it by adjusting the calorimeter position. Typical values are in the order of ± 0.05 mm.

- δ_η: relative miscalibration between the up and down channels of the calorimeter, see section 5.3.3. Typical values are in the order of ± 0.005.

- C_1, C_2, λ_1, λ_2, λ_3: parameters of the η–y–transformation, see equation 25.

- a: parameter a of the energy resolution, see section 5.2. Since this parameter is also determined during the energy calibration it is not necessary to use this fit parameter.

- N: overall normalisation of the histogram. At the low positrons currents that were used up to now, typically 50000 Compton events are collected during one data taking cycle.

- $(S_1^R + S_1^L)/2$: sum of the linear laser polarisation components of both helicity states.

- $(S_3^R + S_3^L)/2 \cdot P_{\text{Y}}$: sum of circular laser polarisation components of both helicity states times the beam polarisation. Since $S_3^R + S_3^L$ is very small under normal conditions and the beam polarisation has been zero in the most data samples taken up to now, this parameter has been fixed to zero.

- f_E: overall factor applied to the energy calibration. This parameter is chosen to 1 by the fit, showing that the energy calibration from the one-dimensional spectrum is valid.

- f_η: factor allowing to scale the function $s^2(E, \eta)$ of the η resolution determined from the GEANT simulation (see section 5.2). This parameter doesn't improve the χ^2/d.o.f. of the fit and comes out to be equal to one, therefore it is usually fixed.

- Δz: distance between Compton interaction point and the calorimeter surface. In case the η–y–transformation is fitted, this parameter is redundant. When however the positron beam moves and the laser beam is accordingly readjusted, the z–distance is actually expected to change, whereas the η–y–transformation should in principle stay unchanged. Therefore this parameter is used in fits with reduced number of parameters when the η–y–transformation is fixed.

After the limited experience collected with the new system up to now, a usefull reduced mode varies only the beam spread, the y–offset, the η–offset, the normalisation, the linear polarisation and the z–distance. In this case, the η–y–transformation needs to be known from previous runs under similar conditions. From time to time, especially for each new run period, the η–y–transformation should be measured with the full fit before the reduced fit is applied. Much more polarised data are needed before a final procedure can be defined.

At first sight it is surprising to see that a fit with 14 parameters actually converges and produces a meaningful result.

The first reason that this procedure works is the high statistics that is available. Approximately 2000 η/E bins are used in the fit, each containing on average 300 events. Therefore, approximately 2000 measurements with an accuracy of $1/\sqrt{300} = 6\,\%$ enter the fit. The second reason is that all fit parameters that are used have a unique effect on the shape of the fit function.

Fitting the η–y–transformation

Most surprising is probably that the fit is able to determind the shape of the η–y–transformation, without making use of testbeam data. This becomes plausible if one takes into account that the Compton scattering cross-section at fixed energy E has two sharp Jacobian peaks at $y = \pm R\,(E)$. Even with the finite η resolution of the calorimeter, this leads to a double–bump structure of the measured η spectrum for a given energy slice (see Fig. 12). The position of these bumps can in fact be plotted against the y peak position to give a rough estimate of the η–y–transformation. For this reason, the fit is also able to extract the η–y–transformation, and at the same time takes into account effects from the finite energy and η resolution.

A numerical problem arises, because the parametrisation Eq. (25) can have very similar values in the y range of interest, i. e. $|y| < 4\,\text{mm}$, for very different sets of parameters, so that the fit can fall in one of several nearly equivalent minima of the χ^2 function. This can be overcome by chosing a preferred value for one of the parameters and adding a corresponding term to the χ^2, so that the fit tends to choose always the same minimum.

The overall χ^2 of the fit depends strongly on the η–y–transformation, which is indicated by the fact that a parametrisation with only two exponentials (i. e. $C_2 = \lambda_3 = 0$) is not sufficient to describe the data satisfactorily.

The η–y–transformation is the most important input for the online analysis, which is obvious from the fact that a mean value of η is measured in this method. Monte Carlo studies indicate that shower shapes from electrons and photons are sufficiently different to affect the η–y–transformation in a measurable way. The η–y–transformation also depends on whether a photon has interacted in the preradiator or hits the calorimeter surface intact.

Therefore it is advantageous to adapt the η–y–transformation such that it fits the measured data optimally, as is done by the fit method.

Fitting beam spread versus linear light polarisation

Two parameters that have similar effect on the fit function are the linear light polarisation terms $(S_1^R \pm S_1^L)/2$ and the beam spot size σ_{y}.

Eqs. (10) and (11) show that the linear polarisation corresponds to a term proportional to $\cos 2\phi$, which is maximal at $\phi = 0$ and maximally negative at $\phi \pm \pi/2$, which corresponds to $y = \pm R(E)$. Therefore, a linear polarisation component enhances or depletes the bumps in the η spectrum. For the online analysis, this leads to a dilution of the η shift between the left and right handed data, therefore to a change in the analysis power.

The effect of the beam spread is a broadening of the bumps in the η spectrum, which for the online method also changes the analysing power.

At any single energy, the effect of linear laser polarisation and the beam spread are difficult to disentangle. However, the energy dependence of the linear polarisation terms, given by Σ_1 in eqs. (10) and (11), is different for the linear laser polarisation term and the unpolarized term Σ_0. This differnce makes it possible to disentangle the two effects reliably.

Fitting a y offset versus a gain difference

If the calorimeter is not perfectly centered with respect to the photon beam, the y coordinate y_{calo} measured by the calorimeter does not coincide with the true value y_{beam}. If one plots η versus y_{beam}, as in Fig. 9, such an offset corresponds to a horizontal shift of the whole η–y–transformation. A y offset $\delta y = y_{\mathrm{calo}} - y_{\mathrm{beam}}$ of the calorimeter and a difference in energy response of the upper and lower halves of the calorimeter both affect the mean η value for a given energy range. To zeroth order, both shift the η spectrum by a certain amount. But since the fit method determines the complete η–y–transformation, it is sensitive to the quite different ways in which the two offsets change this transformation, as shown in Fig. 9. Therefore, the fit can very well distinguish between both effects.

5.3.5 The Polarisation Fit

The polarisation fit varies only two parameters:

- $(S_1^R - S_1^L)/2$: difference of linear laser polarisation components of both helicity states.

- $(S_3^R - S_3^L)/2 \cdot P_{\mathrm{Y}}$: difference of circular laser polarisation components of both helicity states times the beam polarisation.

These parameters can be distinguished easily by the fit, since the corresponding cross section terms are an even function of η (or ϕ) in case of the linear laser polarisation and an odd function in case of the beam polarisation (see also equation 7). All other parameters are fixed to their values obtained from (or used in) the calibration fit.

5.3.6 Estimating the Circular Laser Polarisation

The difference of the circular laser polarisations, $(S_3^R - S_3^L)$, cannot so easily be disentangled from the beam polarisation. There are two ways to get an estimate on this quantity. First there is the possibility to measure degree and direction of the linear component of the laser polarisation with a Glan prism as described in [2]. But since the laser polarisation measurement can not be done without adjusting the mirrors differently than for the beam polarisation measurement it is not completely clear if the linear light component measured with the prism is actually the same as in the beam polarisation measurement. The second way to estimate the circular laser polarisation is to use the size of the correspondant linear components as measured together with P_Y. In this case however only the vertical component is measured and thus only an upper limit on the circular laser polarisation can be obtained.

5.4 Application to Data

The overall performance of the full fit on a data set from a single one–minute cycle is shown in figure 10. The left column is dedicated to the calibration fit, while the right column shows the polarisation fit. In both cases the data spectra are displayed in the upper plot. The histogrammed fit function at the end of the fit can be seen in the middle and the binwise pull, defined as $(DATA - FIT)/\delta DATA$, is shown in the lower plots. The right column contains the same three plots for the difference of both laser helicity states. The beam polarisation was about 20%. The fit range which includes approximately 2000 bins is indicated by the red box. The remarkable description of the data by the fit is further illustrated in figure 11 for the calibration fit and in figure 12 for the polarisation fit. Each show three energy slices out of the corresponding two–dimensional histograms of figure 10. The left column shows data (black dots with error bars) and fit result (green line) together. In the right column, the relative difference of the two is displayed. The data were taken with a positron current of about 9 mA, which is a factor 5 to 6 below HERA II design. Thus, the statistical precision for the full HERA II currents will be considerably better.

A more quantitative statement can be derived from the frequency distributions of the binwise pulls, which are shown in figure 13 for the calibration (left) and polarisation (right) fit on the same data as used in the previous figures. Each bin within the fit range gives one entry in the pull distribution. A perfect fit should yield a gaussian distribution with a mean of zero and a width of one. Both fits come very close to that goal. With a value of 1.05 ± 0.02, which corresponds to a χ^2/d.o.f. of 1.17, the pull distribution of the calibration fit is slightly too broad.

While the performance of the fit up to now has been illustrated on a single data taking cycle, figure 14 shows the χ^2/d.o.f. for more than 1000 one–minute cycles taken on March 1, 2003 when up to 50% polarisation was achieved[3]. The average χ^2/d.o.f. of the polarisation fits is 1.02. The average χ^2/d.o.f. of the calibration fits is with 1.12 slightly larger, but still very good. Since this slightly higher average χ^2/d.o.f. is not observed in Monte Carlo simulations, it indicates that the understanding of the polarimeter and thus the precision of the analysis could be improved even further.

[3]HERA fill 3188

The measured polarisation for the same data averaged over five cycles is shown in the upper part of figure 15. The online (open squares) and offline analysis (full dots) agree quite well in general, but small differences in both directions can be seen. Note that also the statistical precision is improved by the offline analysis w.r.t. the online method, which is further illustrated by the lower plot. Errors increase with time as the positron current in the ring decreases. Sometimes the Compton luminosity can be increased again by readjusting the laser beam.

5.5 Monte Carlo Studies

A number of checks have been performed using Monte Carlo simulations. By varying one of the system parameters and applying online and offline analysis, the influence of each parameter on the beam polarisation measurement can be extracted. Although no final number can be quoted before more data has been accumulated, the results of four of the simulations are presented here to illustrate the improvement. Each simulation comprises 100 one–minute cycles[4], and in each simulation one of the key parameters is changing with time, usually over a much wider range than expected in the real measurement. The positron current was assumed to be about 20 mA, which is significantly below HERA II design but twice as much as in the only polarised data available sofar. In each of the following figures the green line indicates the input values to the simulation, while the red line shows a fit to the values reconstructed by the fit method, which are displayed as black dots with error bars. For quantities accessible to the online analysis (especially for the beam polarisation), the corresponding online results are shown as open blue squares for comparison.

- Fig. 16: The linear polarisation component of the left handed laser state is increased from 0 to 50% (upper left), while the linear component of the right handed laser state remains constant at 15% (upper right). The offline fit traces very well the resulting changes in $S_1^R + S_1^L$ (middle left) and $S_1^R - S_1^L$ (middle right). The latter quantity can also be extracted by the online analysis, which in this case also works well, although with a slightly too shallow slope. The beam polarisation determined by the fit agrees within $\delta P_{\mathrm{Y}}/P_{\mathrm{Y}} = 0.25\%$ with the constant simulated value of $P_{\mathrm{Y}} = 0.65$ (lower left), while the online value (lower right) is obviously influenced by the change of linear polarisation.

- Fig. 17: Here the vertical offset between calorimeter center and beam axis is varied from 0 to 0.1 mm (upper left), while the linear components of the two laser polarisation states remain constant (middle). The variation of the vertical offset is traced perfectly by the fit, while the online analysis underestimates the offset. To compensate, the online analysis decreases the difference of the linear laser polarisation components $S_1^R - S_1^L$ (middle left) and increases the beam spot size (upper right). The effect on the beam polarisation measured online is however small, although it is too high overall (lower right). This illustrates the fact that the online analysis assumes some fixed η–y–transformation, which happens to be different from the one used in the MC simulation. The beam polarisation from the fit, which adapts the η–y–transformation such that it describes the simulated data, agrees within $\delta P_{\mathrm{Y}}/P_{\mathrm{Y}} = 0.45\%$ with the simulated value.

[4]only the Compton signal is simulated, not the background

- Fig. 18: This simulation has the same variation of the vertical offset as the previous one. However the functional shape of the η–y–transformation transformation which enters the simulation has been chosen differently, while the parametrisation used in the fit is the same as usual. Although the results look very similar to those in figure 17 a larger difference between online and offline results for vertical offset (upper left) and beam spot size (upper right) can be observed. The online beam polarisation (lower right) is closer to its simulated value, which indicates that the alternative η–y–transformation used here is closer to the one that was assumed when the analysing power for the online method was calculated. While the fit result for the beam polarisation (lower left) is as good as in the case shown in 17, the beam spread (upper right) and the sum of the linear laser polarisation components (middle left) seem to differ slightly from the simulated values, which should be investigated further in the future.

- Fig. 19: In this simulation the relative miscalibration of the calorimeter's up and down channels is increased from 0 to 10%. The change is correctly recognised by the fit (upper left) and can clearly be distinguished from a change in vertical position (upper right) or a change in the beam spot size (middle left). The fit also reconstructs the difference of the linear laser polarisation components correctly (middle right), while the online analysis compensates the miscalibration with artificial changes in these quantities. These mismeasurements don't have a strong effect on the online beam polarisation measurement itself, but a clear slope can be seen nevertheless (lower right), whereas the fit method reconstructs the simulated polarisation values within 0.2% (lower left). It has to be stated clearly that the true online situation is much better, since the run control would readjust the photomultiplier gains in case the miscalibration, which is monitored using the "left" and "right" channels of the calorimeter, gets significant.

- Fig. 20: Here the vertical beam spot size at the calorimeter surface is varied from 0.25 mm to 0.75 mm. Again the fit resolves all parameters correctly. Especially the beam polarisation agrees with the simulated value within 0.25% (lower left). In contrast to the previous cases, the online polarisation measurement is heavily affected. Although the range of variation applied here is larger than what is expected in reality, it shows the importance of knowing and taking into account the optics.

- Fig. 21: In this case several parameters have been varied simultaneously and in a more realistic range: 0.25 mm $< \sigma_y <$ 0.35 mm, 0.05 mm $> \delta_y > -0.05$ mm, $0 < \delta_\eta < 0.05$, $10\% > S_1^R > 0$, $-5\% > S_1^L > -5.5\%$. It can be seen clearly that the fit can disantangle very well all the different changes. The fitted polarisation value agrees within 0.1%. It is interesting to note that the online analysis measures the vertical offset with a slope of opposite sign, leading to a situation where even the offset values themselves get the wrong sign.

- Fig. 22: Here we have the same situation as in figure 21, but additionally all five parameters of the η–y–transformation are varied within sensible values. Again, the fit can resolve the parameter changes correctly and measures a beam polarisation which agrees with the simulated value within 0.2%.

These examples illustrate the performance of the new fit method. In most cases they exaggerate the changes far beyond the real expectation, since the run control measures several parameters which allow to readjust the system in case a deviation becomes too large. One interesting parameter however is the beam spot size, which was varied in the simulation shown in figure 20. It depends not only on the vertical α– and β–functions, but also on the emittance of the beam and the exact position of the Compton interaction point, which might vary if the positron or the laser beam is adjusted. As figure 20 shows, the online analysis has difficulties to determine this parameter correctly. Also in the available data online and offline measurement often disagree on the size of the beam spot. Additionally, this quantity has a non–negligible impact on the analysing power used in the online measurement, as can be seen from the slope of the online polarisation measurement in figure 20.

The other key issue is the knowledge of the η–y–transformation. Although it is expected to be time independent (or at least only slowly changing due to radiation influence on the scintillators in the calorimeter), it has to be known precisely to derive a correct analysing power for the online measurement, as can be seen from the slope of the online polarisation measurement in figure 22, where the η–y–transformation parameters were varied in the simulation.

In all cases, the fit traces the parameter changes correctly even if several parameters are varied at the same time and it reproduces the simulated polarisation within $({P_\mathrm{Y}}^{\mathrm{fit}} - {P_\mathrm{Y}}^{\mathrm{sim}})/{P_\mathrm{Y}}^{\mathrm{sim}} \leq 0.5\%$. Although these studies have to be repeated with real data, they show that the new analysis presents a substancial improvement in the understanding the polarimeter.

6 Summary

With the luminosity upgrade at HERA, a longitudinally polarised lepton beam is provided not only to HERMES, but also to H1 and ZEUS. Since the physics programme of the collider experiments requires a polarisation measurement with a relative precision $\delta P_\mathrm{Y}/P_\mathrm{Y}$ of 1% or better, the Transverse Polarimeter as been upgraded substancially. Besides a new data acquisition system, and a new silicon strip detector for calibrating the position measurement of the calorimeter, a completely new offline analysis of the calorimeter data has been developed. Its goal is to determine the polarisation without prior assumption on the system parameters, like the η–y–transformation or the beam spot size. This has been achieved by perfoming a fit of the double–differential Compton cross section folded with the detector response to the two–dimensional spectra in energy and position of the scattered photon as by the calorimeter. In a first step, the system parameters are determined from a fit to the sum of the spectra taken with right and left handed circular laser polarisation, in which the effect the beam polarisation cancels. In a second fit to the difference of the same spectra in which the beam polarisation effect is present, all system parameters are fixed to the values found in the first step and only the beam polarisation is varied. The fit has been applied to the data available up to now, especially those taken in March 2003, when HERA delivered up to 50% of longitudinal polarisation to all three experiments after only a few days of tuning. Both the calibration and the polarisation fit describe the data well with an average χ^2/d.o.f. of 1.12 and 1.02, respectively. The performance of the new fit has been studied in detail with Monte Carlo simulations, leading to the preliminary conclusion that the required precision can be achieved. Although these studies have to be repeated with real data, they show that the new analysis presents a substancial improvement in the understanding the polarimeter.

References

[1] A.A.Sokolov, I.M.Ternov, V.V.Mikhailin, Izv. Vuz. Fiz. **4** (1976) 7.

[2] D.P.Barber *et al.*, Nucl. Inst. and Meth. A **329** (1993) 79.

[3] D.P.Barber *et al.*, Phys. Lett. B **343** (1995) 436.

[4] F. James, *MINUIT reference manual (Version 94.1),* Program Library D506, CERN, 1994.

[5] M. Lomperski, *Compton Scattering off Blackbody Radiation and other Backgrounds of the HERA Polarimeter,* DESY 93-045, ISSN 0418-9833.

[6] Application Software Group, Computing and Networks Division, *GEANT reference manual,* Program Library Long Writeup W5013, CERN, 1993.

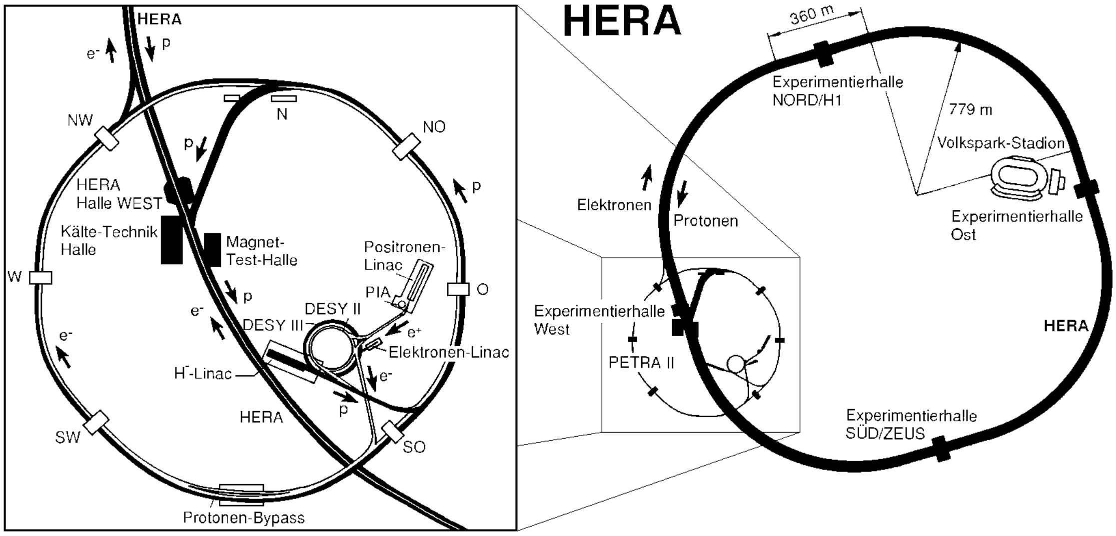

Figure 1: Schematic view of the HERA storage ring and its injector chain. The Transverse Polarimeter is located near hall WEST, approximately 200 m in direction of the north hall.

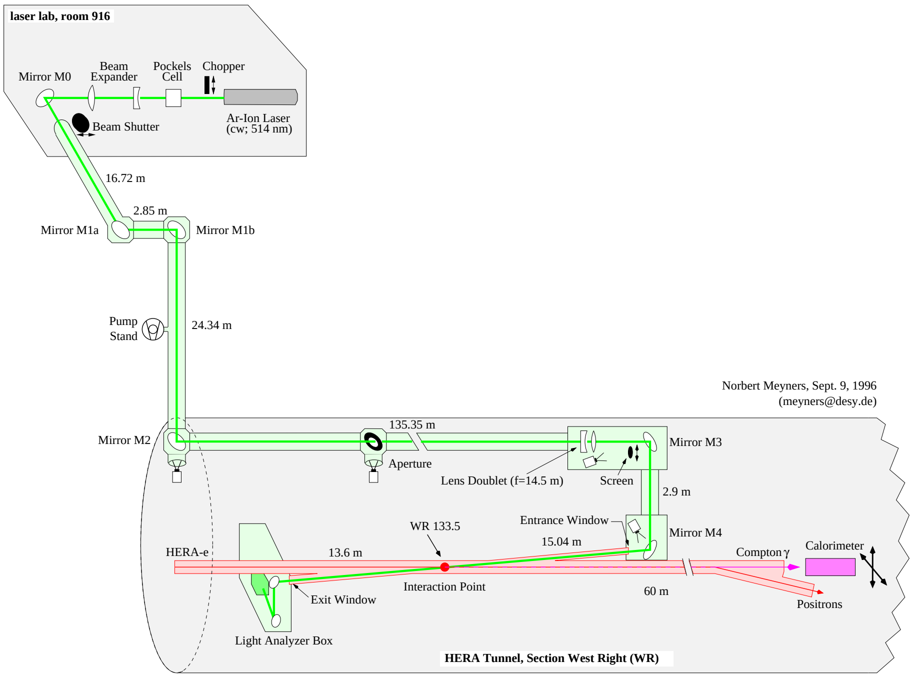

Figure 2: Schematic view of the Transverse Polarimeter including the optical system which guides the laser beam (green line) from the laser room above the west hall into the HERA tunnel. The lepton beam (red line) enters from the left and is hit by the laser beam in the interaction point marked as red dot. The backscattered photons (pink line) travel downstream together with the lepton beam, until the later is bent away by the first dipol magnets of the next arc section. Once separated from the leptons, the Compton photons are detected in the calorimeter.

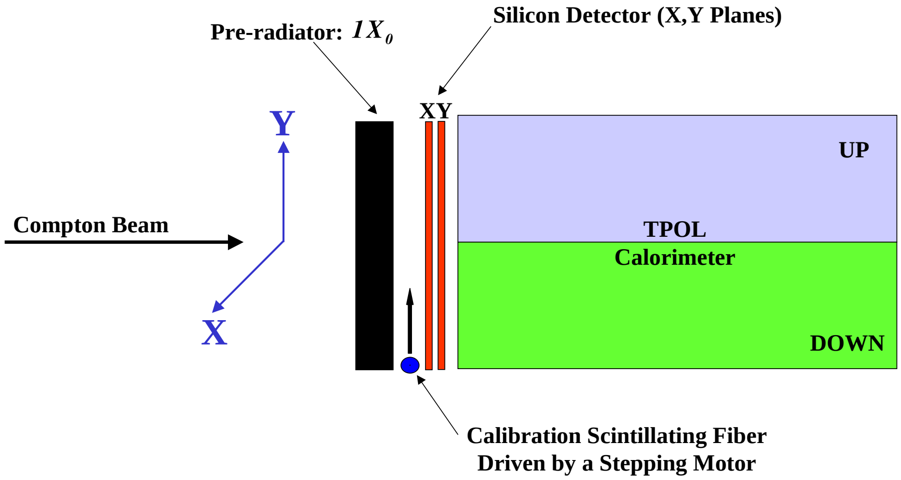

Figure 3: Schematic view of the TPOL detectors. Behind a preradiator of one radiation length lead, photons converted into electron–positron pairs are detected by two single sided silicon strip detectors, one for the x and one for the y coordinate. In order to monitor the local response of the silicon detectors, a scintillating fiber can be moved in front of them. Energy and position of all Compton photons (whether converted or not) are then measured in the tungsten–scintillator sampling calorimeter, which has been described in detail in [2].

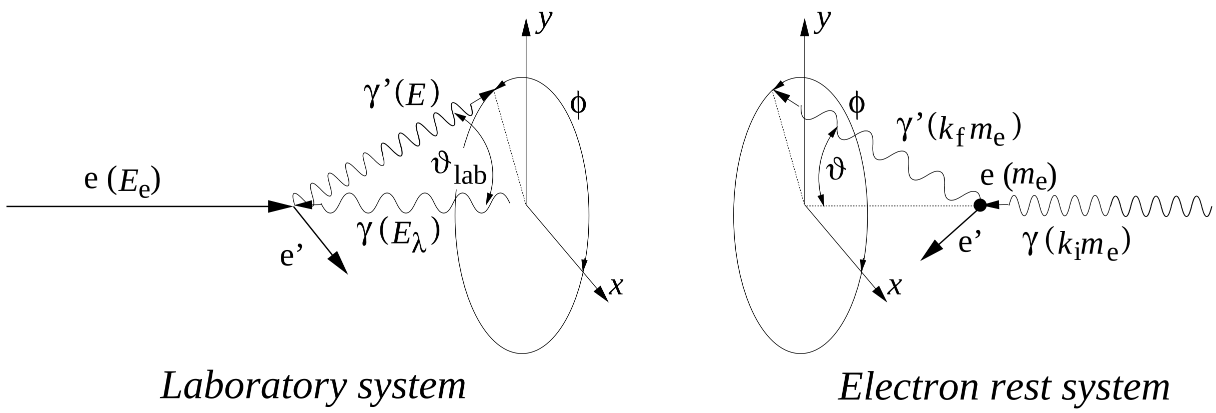

Figure 4: Kinematic of the Compton scattering process in the laboratory frame (left) and in the electron rest frame (right). The notation for the particles' energies as used in the text is given in parathenses.

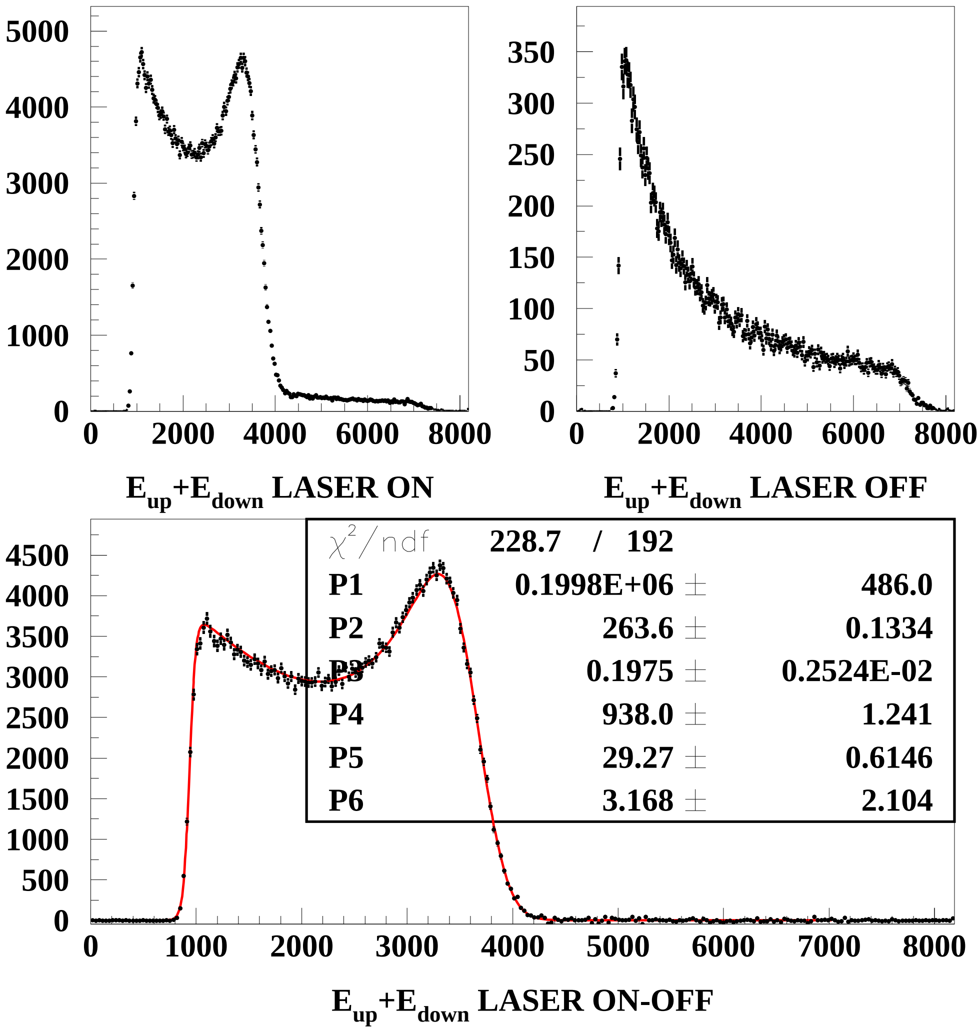

Figure 5: Background subtraction and energy calibration. The upper plots show the energy spectra measured when the laser in on and off. The lower plot shows the corresponding background subtracted energy spectrum with the result of the energy calibration fit. (Meaning of parameters from top to bottom: normalisation, number of ADC counts per GeV, energy resolution, position and width of trigger threshold and remaining background)

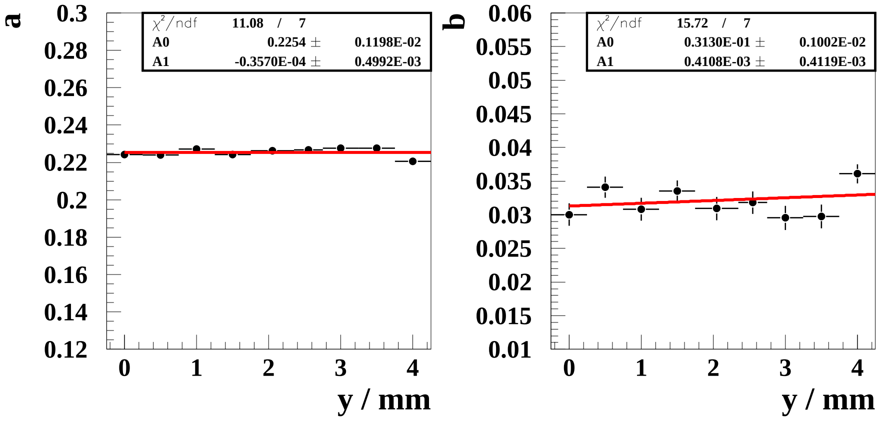

Figure 6: Energy resolution studies using the GEANT simulation: Parameters a (left) and b (right) of the total energy resolution do not depend on the photon's position.

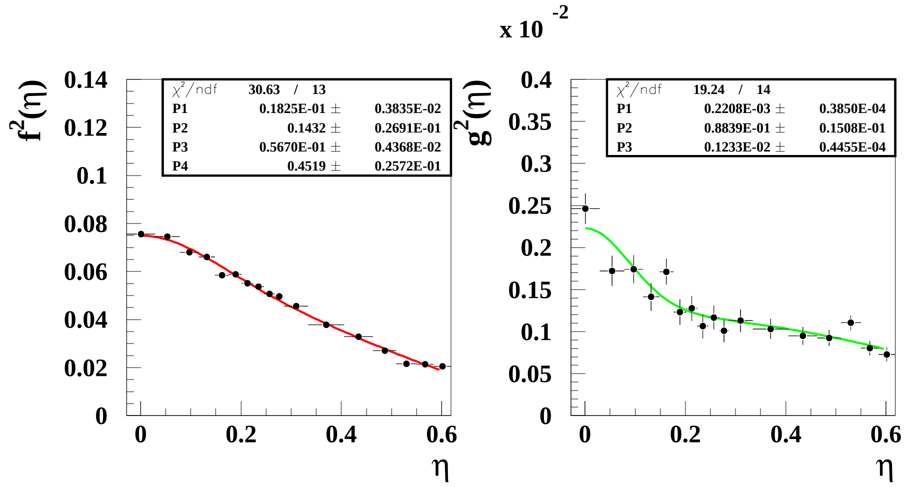

Figure 7: Energy resolution studies using the GEANT simulation: $f^2(\eta)$ (left) and $g^2(\eta)$ (right) as function of η.

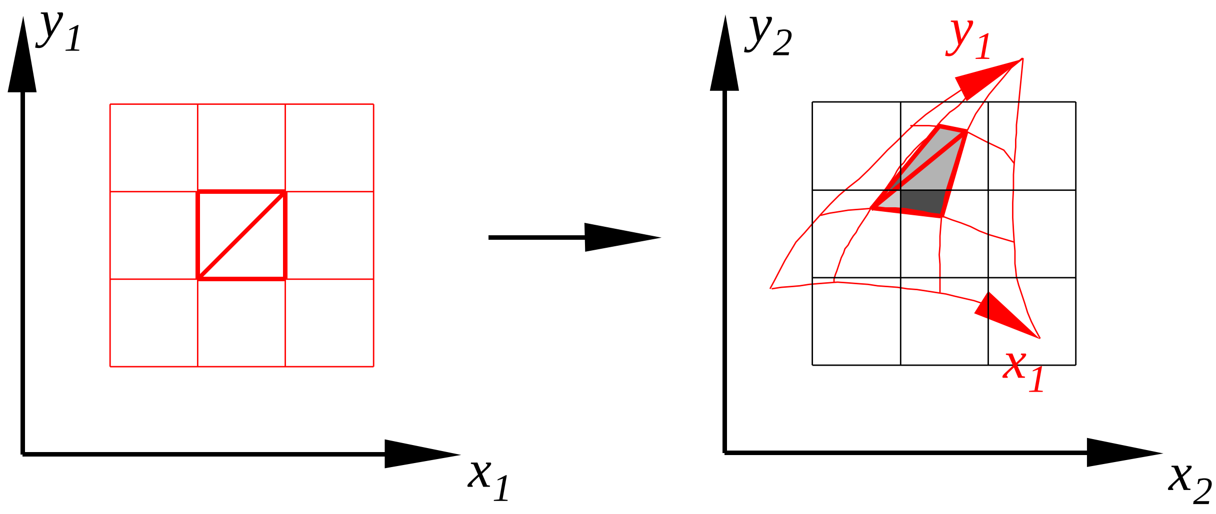

Figure 8: Sketch of the resampling method.

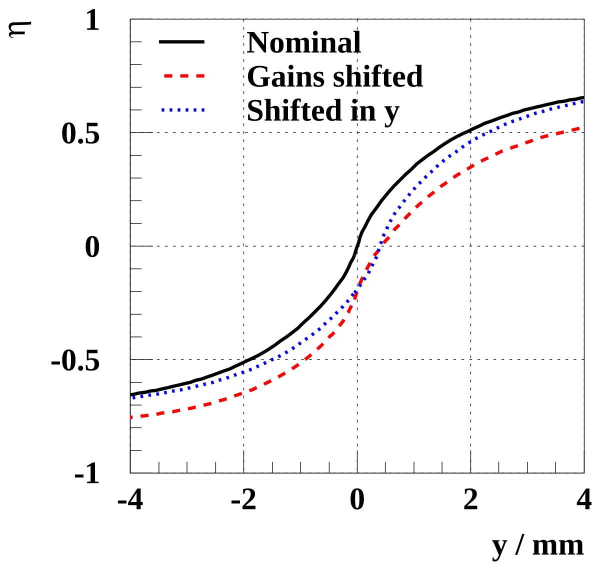

Figure 9: Effect of a y shift of the calorimeter position by 0.5 mm and a gain difference between the photomultipliers of 20 % on the effective η–y–transformation, where y is measured w.r.t. the Compton beam axis.

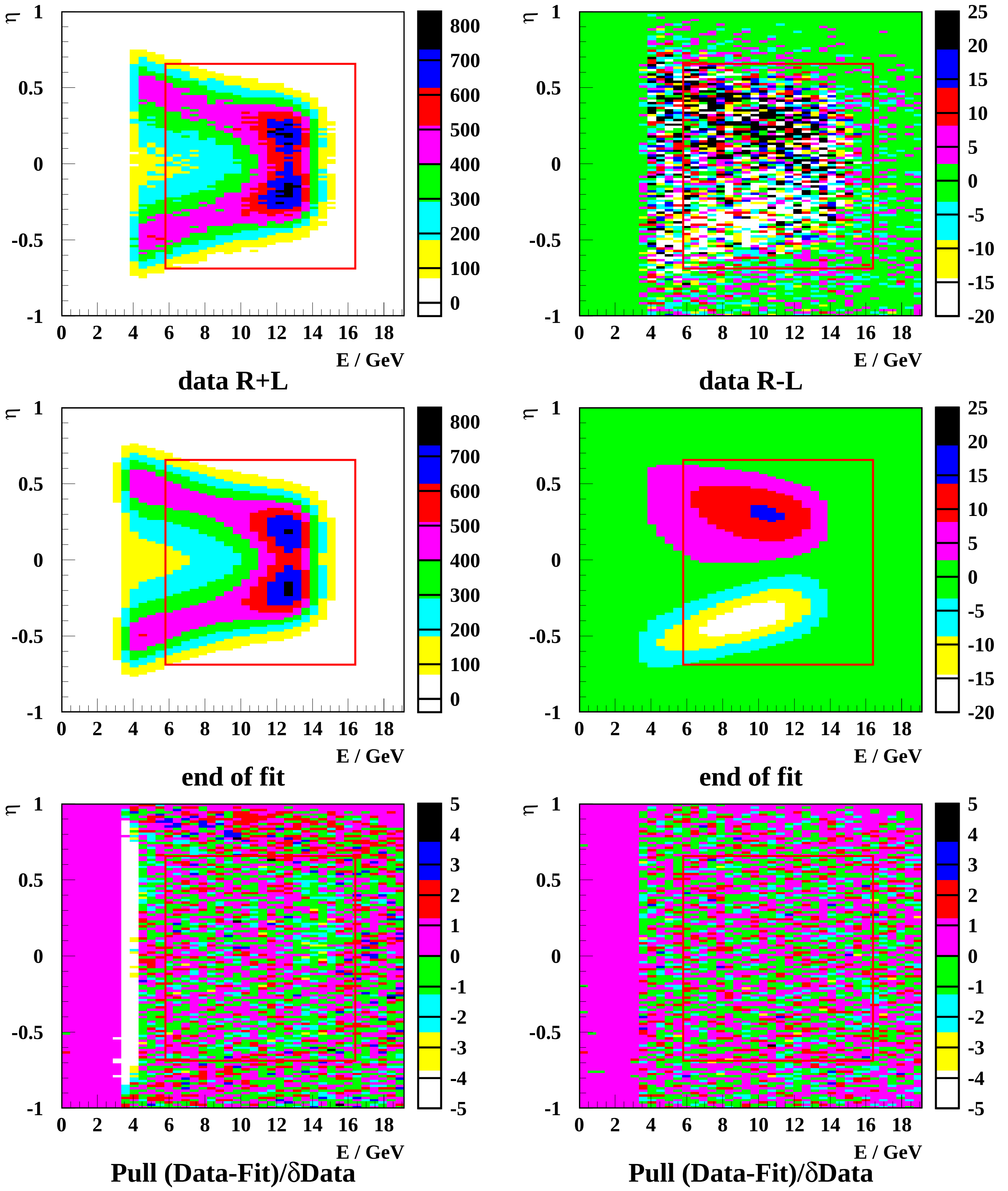

Figure 10: Example of the offline fit on a one–minute data set from October 17, 2002. The left column shows the sum of the data spectra for left and right handed laser polarisation (upper plot), the histogramm fit function at the end of the fit (middle) and the binwise pull (lower plot). The right column contains the same three plots for the difference of both laser helicity states. The fit range is indicated by the red box. It includes approx. 2000 bins.

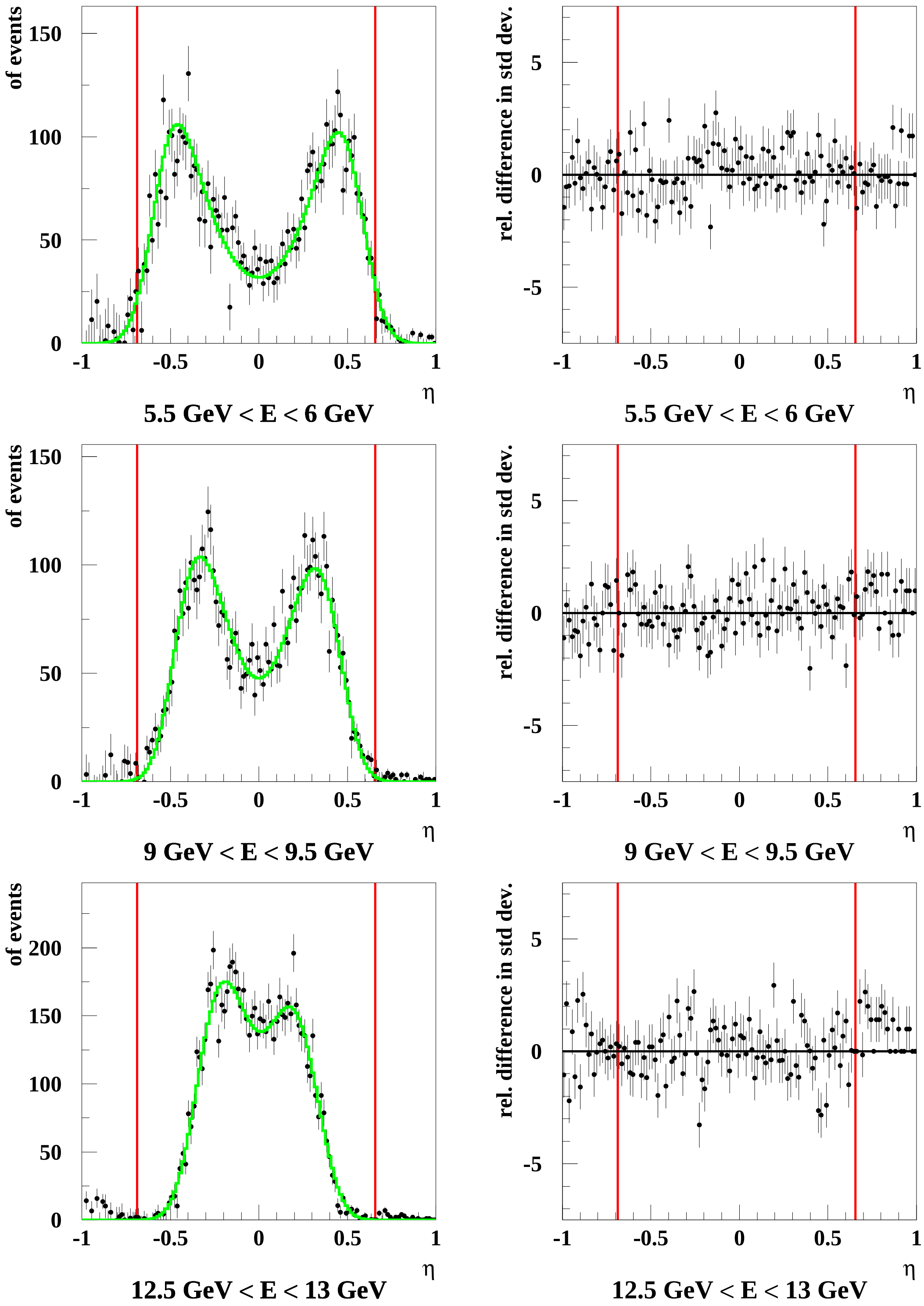

Figure 11: Three energy slices out of the calibration fit shown in fig 10. In the left column, data (black dots with error bars) and fit result (green line) are shown together. In the right column, the relative difference of the two is displayed.

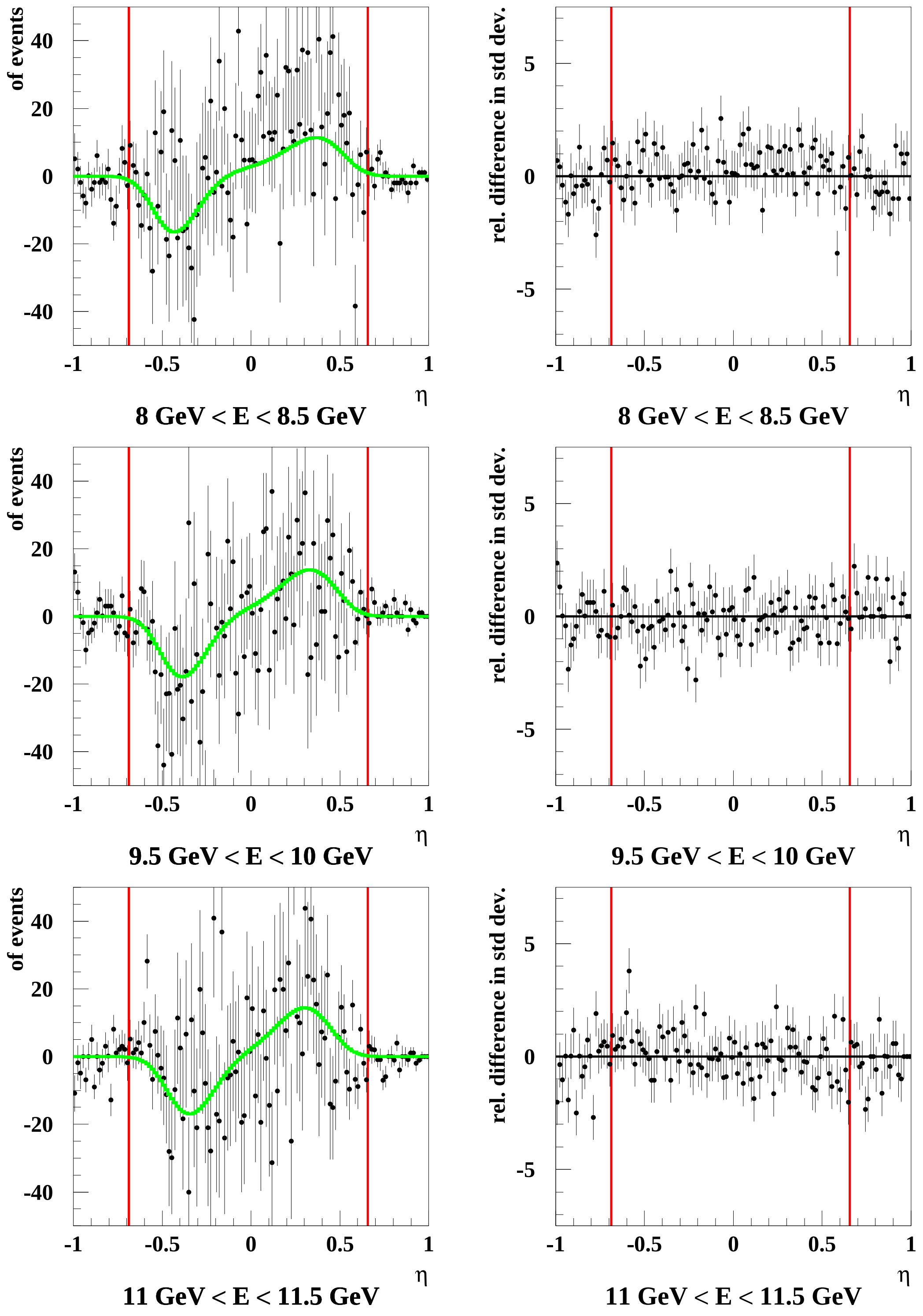

Figure 12: Three energy slices out of the polarisation fit shown in fig 10. In the left column, data (black dots with error bars) and fit result (green line) are shown together. In the right column, the relative difference of the two is displayed. The statistics will improve significantly once HERA runs with design currents.

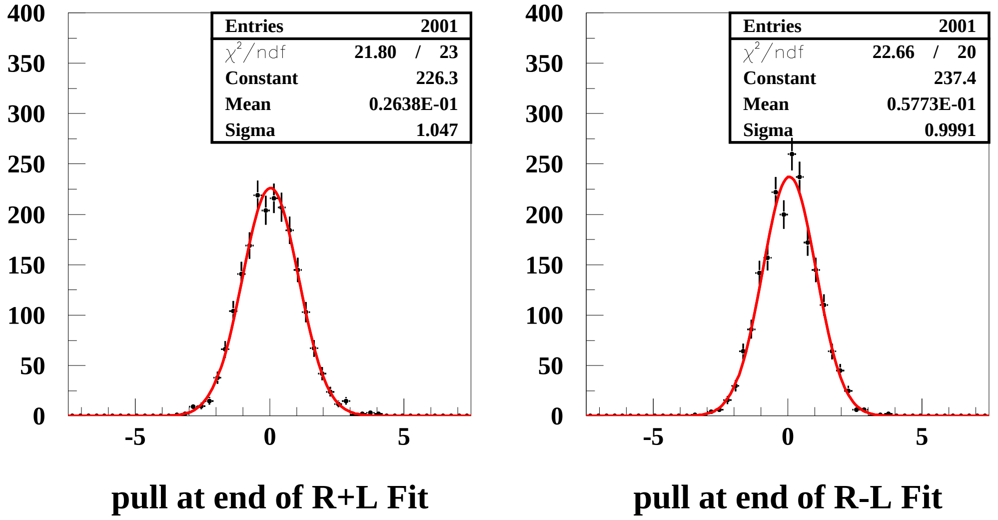

Figure 13: Pull distributions for the fits shown in figure 10 for the calibration fit (left) and polarisation fit (right). The pull of the fits is calculated for each bin inside the fit range and is put as one entry in the histograms shown here. In both cases, the mean of the pull distributions is zero and its width is close to 1 within errors, indicating that the fit discribes the data well.

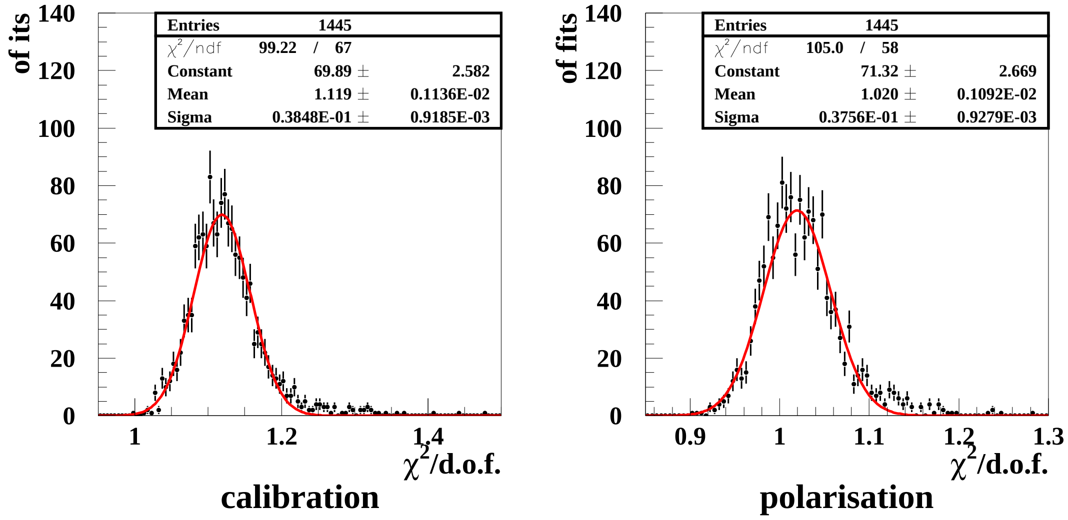

Figure 14: χ^2/d.o.f. for calibration (left) and polarisation fits (right) performed on more than 1000 data taking cycles. While the average χ^2/d.o.f. of the polarisation fits is practically 1, the average χ^2/d.o.f. of the calibration fits is with 1.12 slightly larger, but still very good.

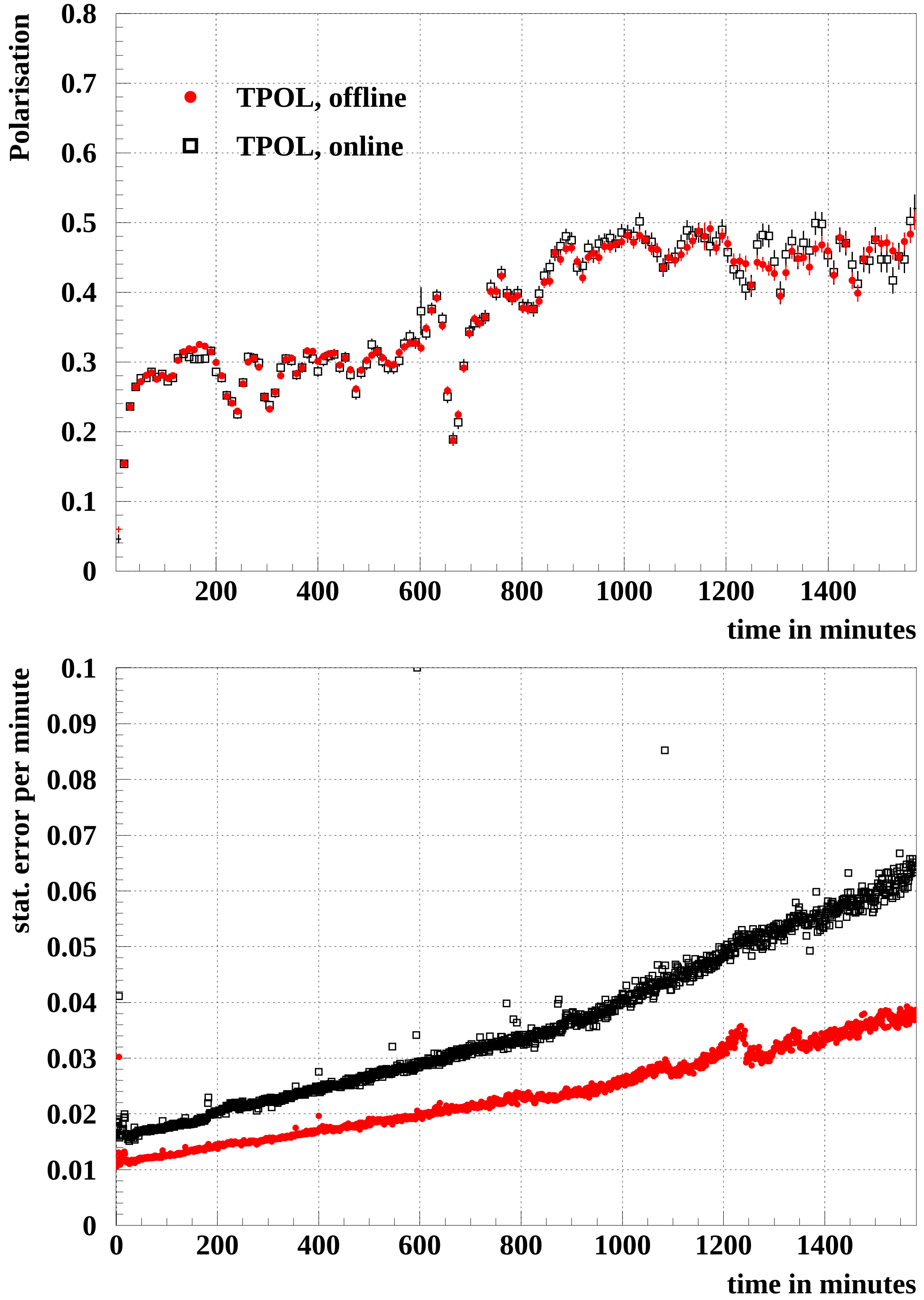

Figure 15: Online (open squares) and offline measurements (full dots) of the beam polarisation during HERA fill 3188 from March 1, 2003, where up to 50% of polarisation was achieved. All three pairs of spin rotators were active.

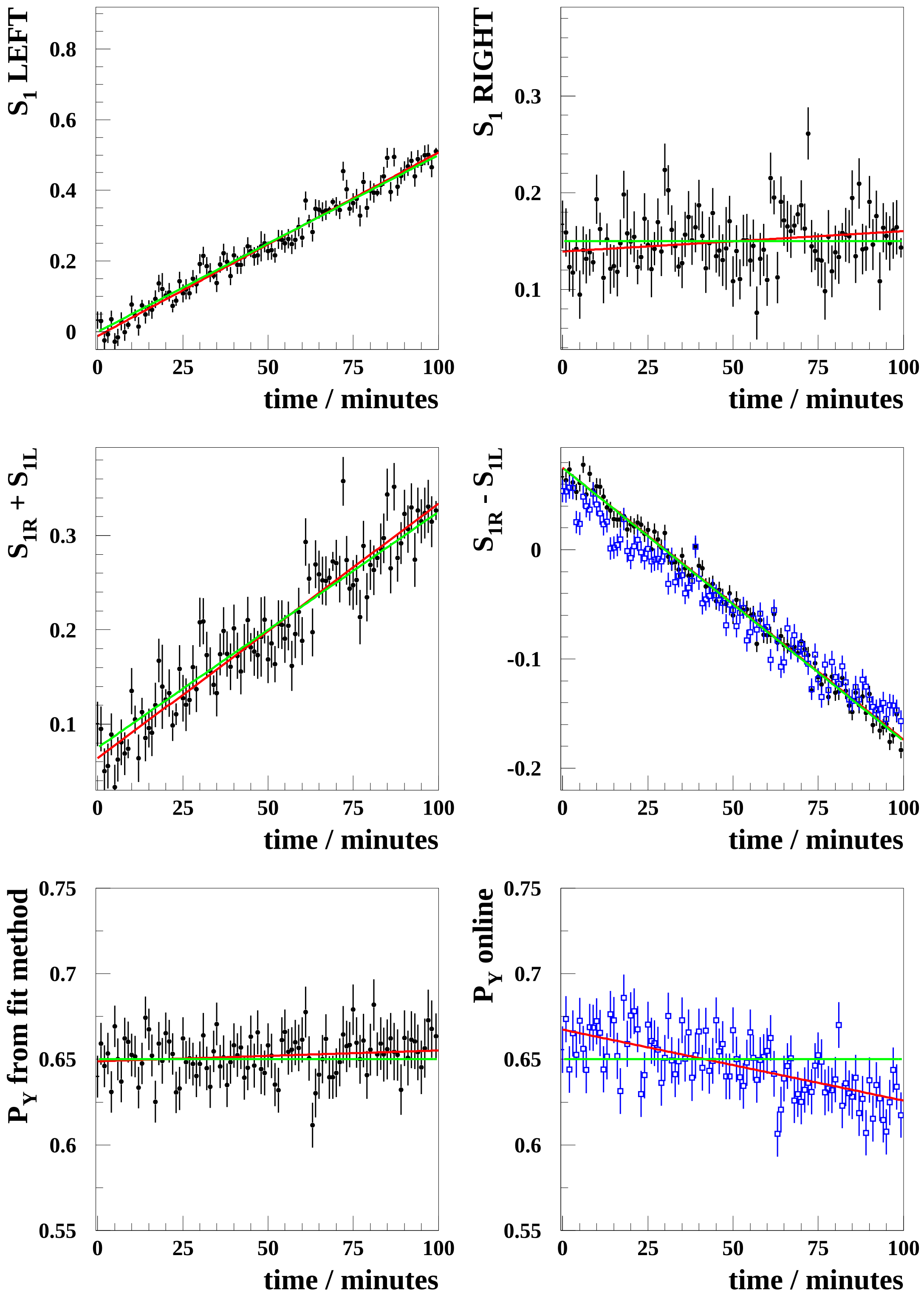

Figure 16: Systematic studies on MC simulations varying the linear polarisation component of the laser: The green line shows the input values of the simulation, while the red line is a fit to the results of the reconstructed values from the new analysis, which are shown as black dots. The result of new analysis for the beam polarisation P_{Y} agrees well with the simulated values. The open blue squares show the results of the online analysis for comparison. For more details see text.

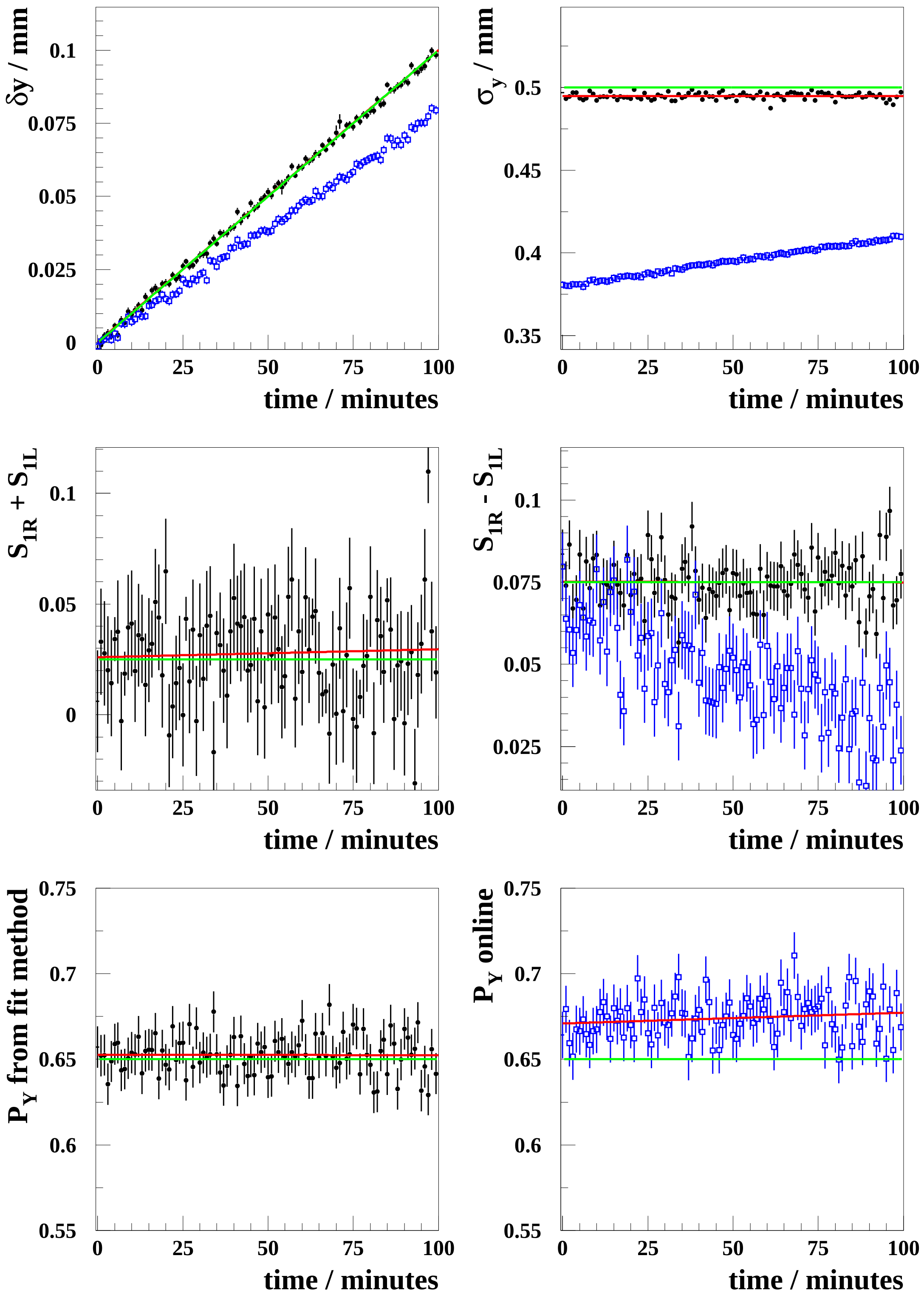

Figure 17: Systematic studies on MC simulations varying the vertical offset between beam axis and calorimeter center: The green line shows the input values of the simulation, while the red line is a fit to the results of the reconstructed values from the new analysis, which are shown as black dots. The result of new analysis for the beam polarisation P_{Y} agrees well with the simulated values. The open blue squares show the results of the online analysis for comparison. For more details see text.

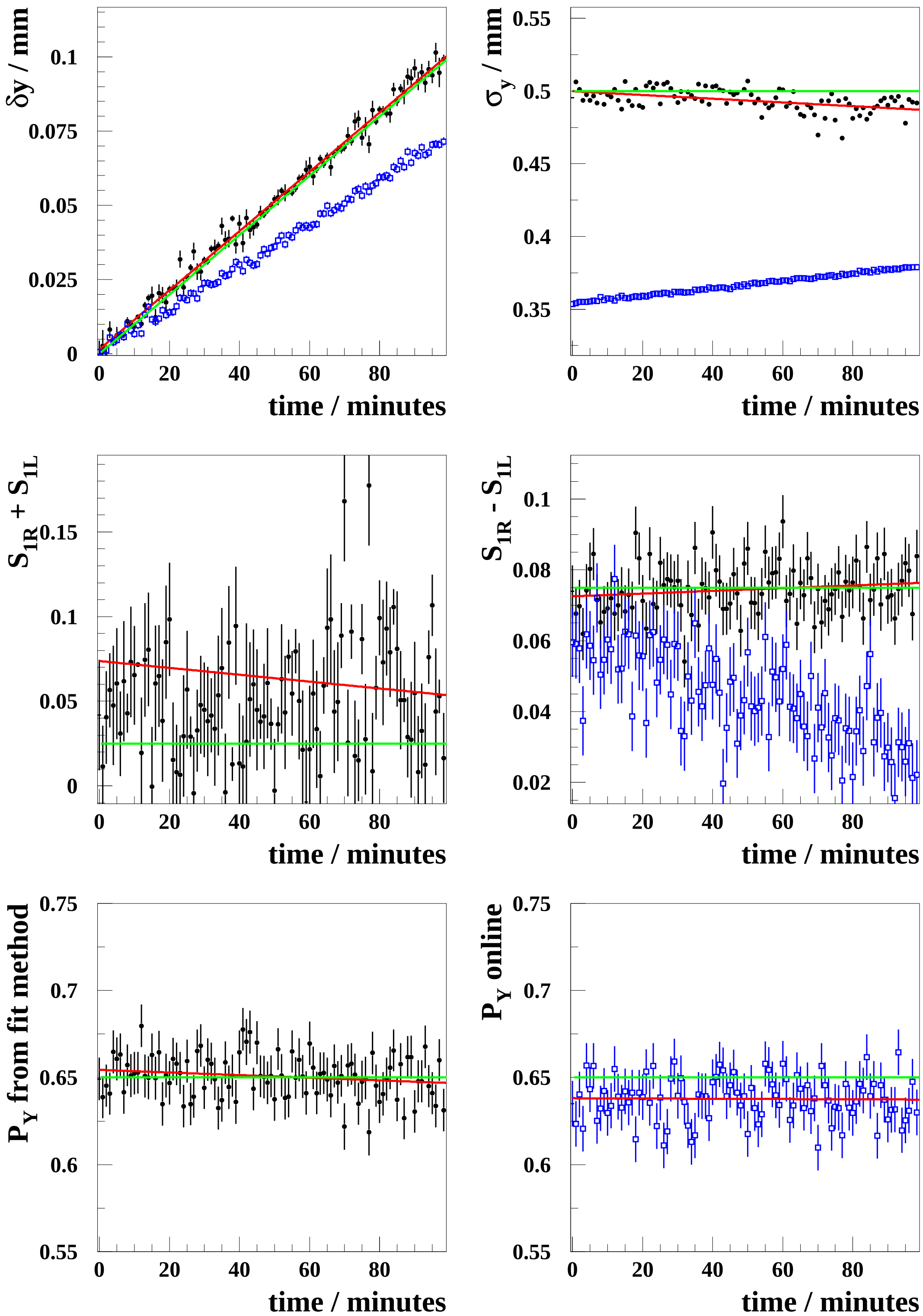

Figure 18: Systematic studies on MC simulations varying the vertical offset between beam axis and calorimeter center and using a different η–y–transformation: The green line shows the input values of the simulation, while the red line is a fit to the results of the reconstructed values from the new analysis, which are shown as black dots. The result of new analysis for the beam polarisation P_{Y} agrees well with the simulated values. The open blue squares show the results of the online analysis for comparison. For more details see text.

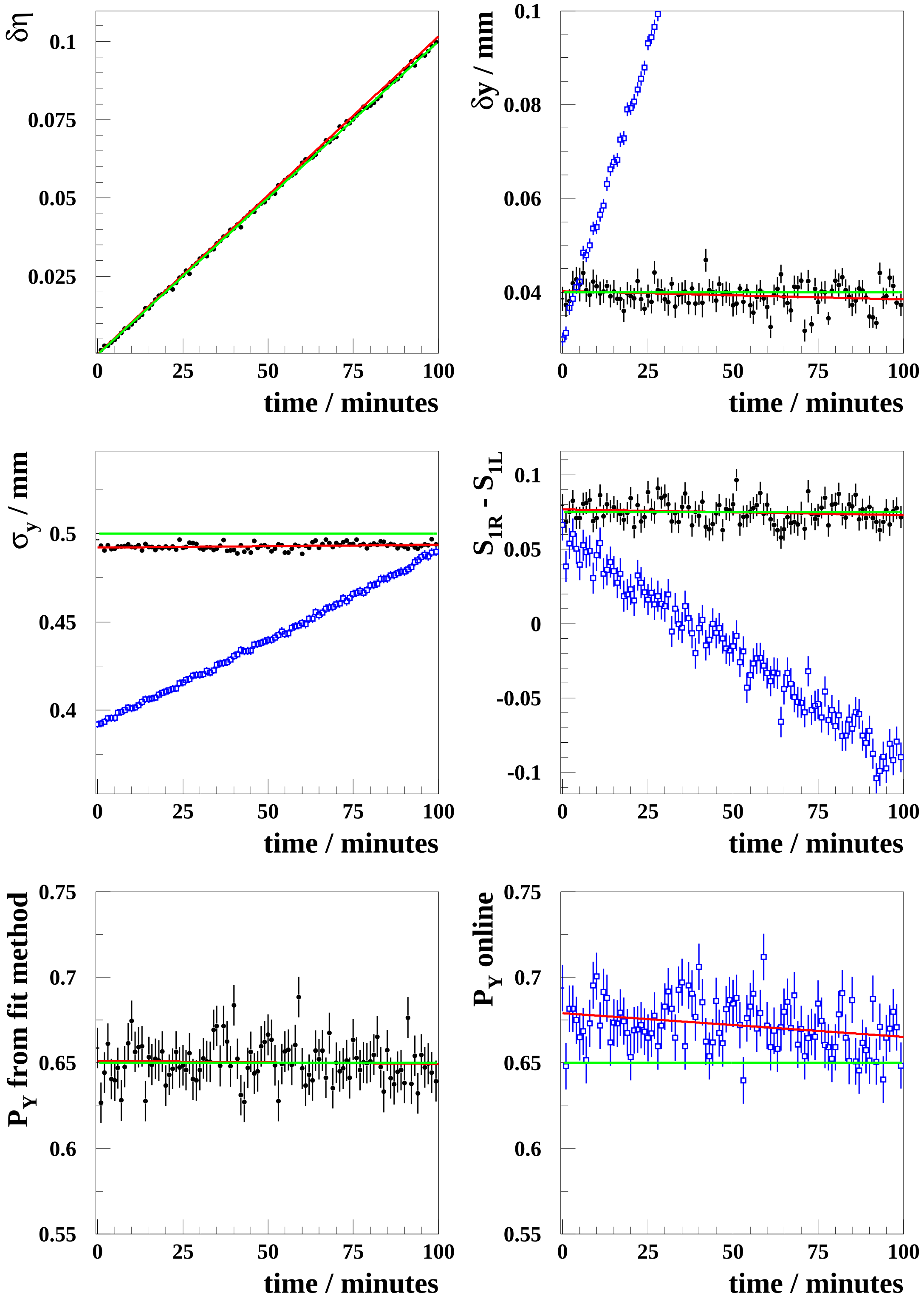

Figure 19: Systematic studies on MC simulations varying the relative miscalibration of the calorimeter's up and down channels: The green line shows the input values of the simulation, while the red line is a fit to the results of the reconstructed values from the new analysis, which are shown as black dots. The result of new analysis for the beam polarisation P_{Y} agrees well with the simulated values. The open blue squares show the results of the online analysis for comparison. For more details see text.

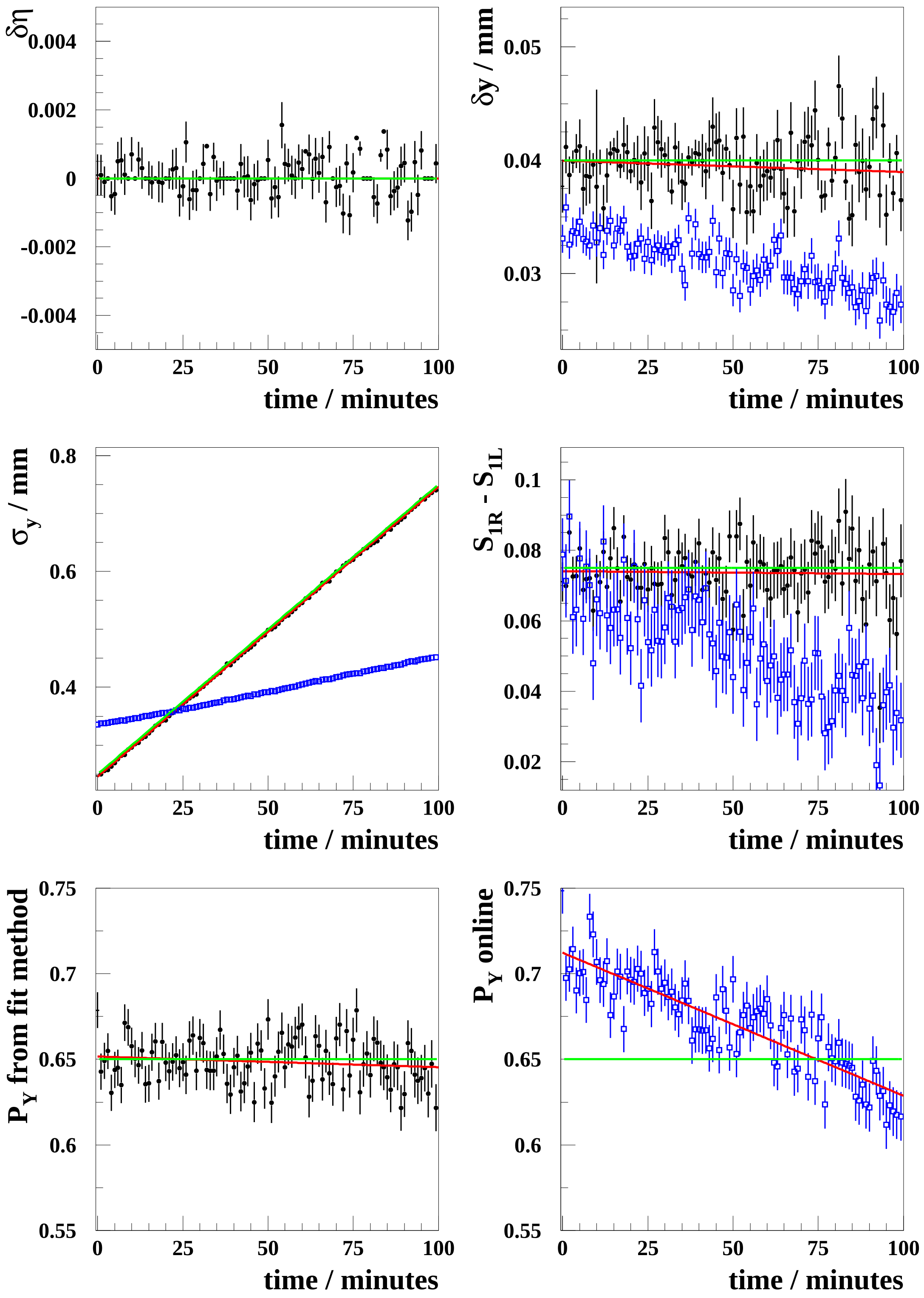

Figure 20: Systematic studies on MC simulations varying the beam spot size: The green line shows the input values of the simulation, while the red line is a fit to the results of the reconstructed values from the new analysis, which are shown as black dots. The result of new analysis for the beam polarisation P_{Y} agrees well with the simulated values. The open blue squares show the results of the online analysis for comparison. For more details see text.

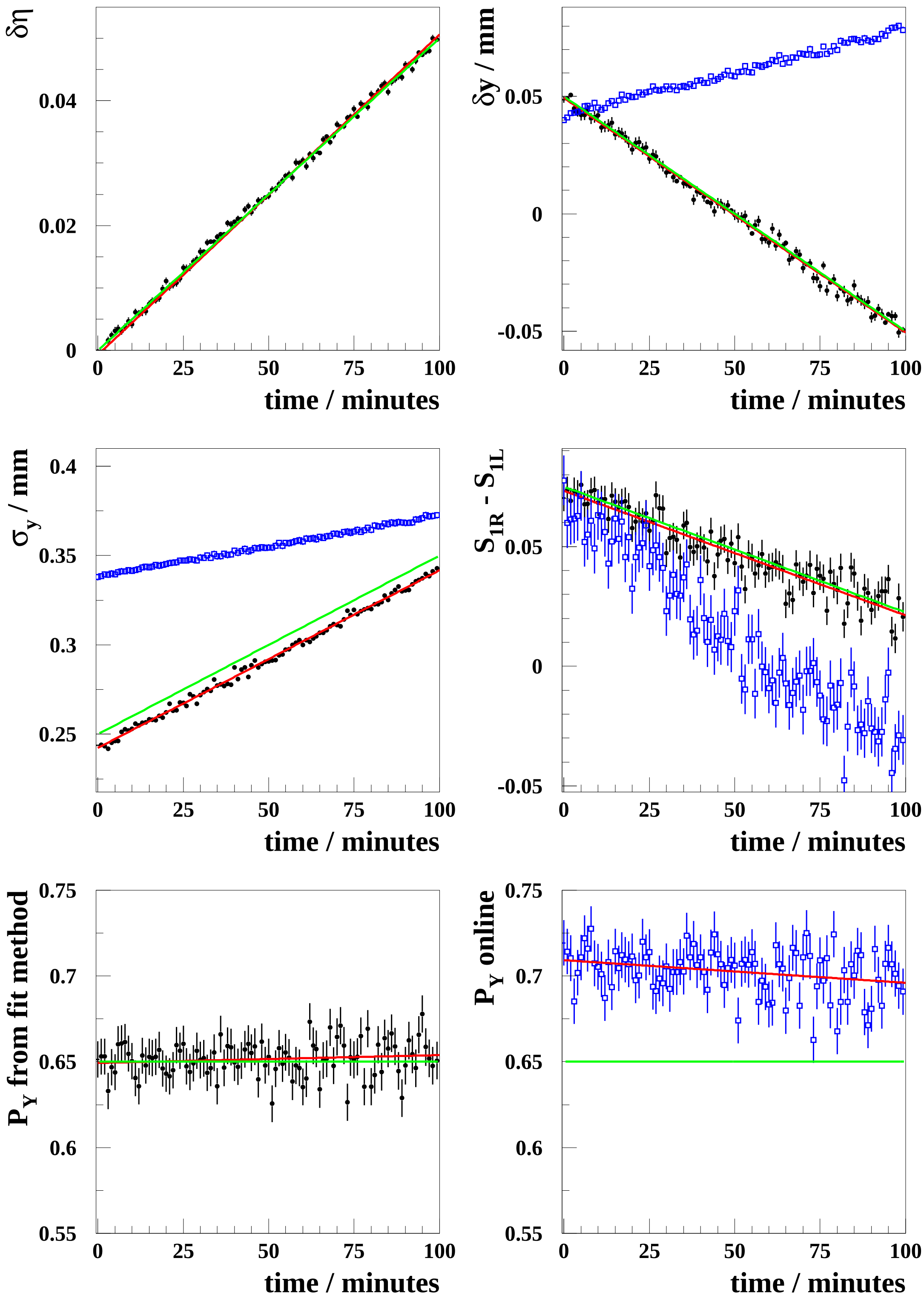

Figure 21: Systematic studies on MC simulations varying the beam spot size, the vertical offset, the relative miscalibration of the calorimeter's up and down channels and the linear polarisation components of both laser helicity states: The green line shows the input values of the simulation, while the red line is a fit to the results of the reconstructed values from the new analysis, which are shown as black dots. The result of new analysis for the beam polarisation P_{Y} agrees well with the simulated values. The open blue squares show the results of the online analysis for comparison. For more details see text.

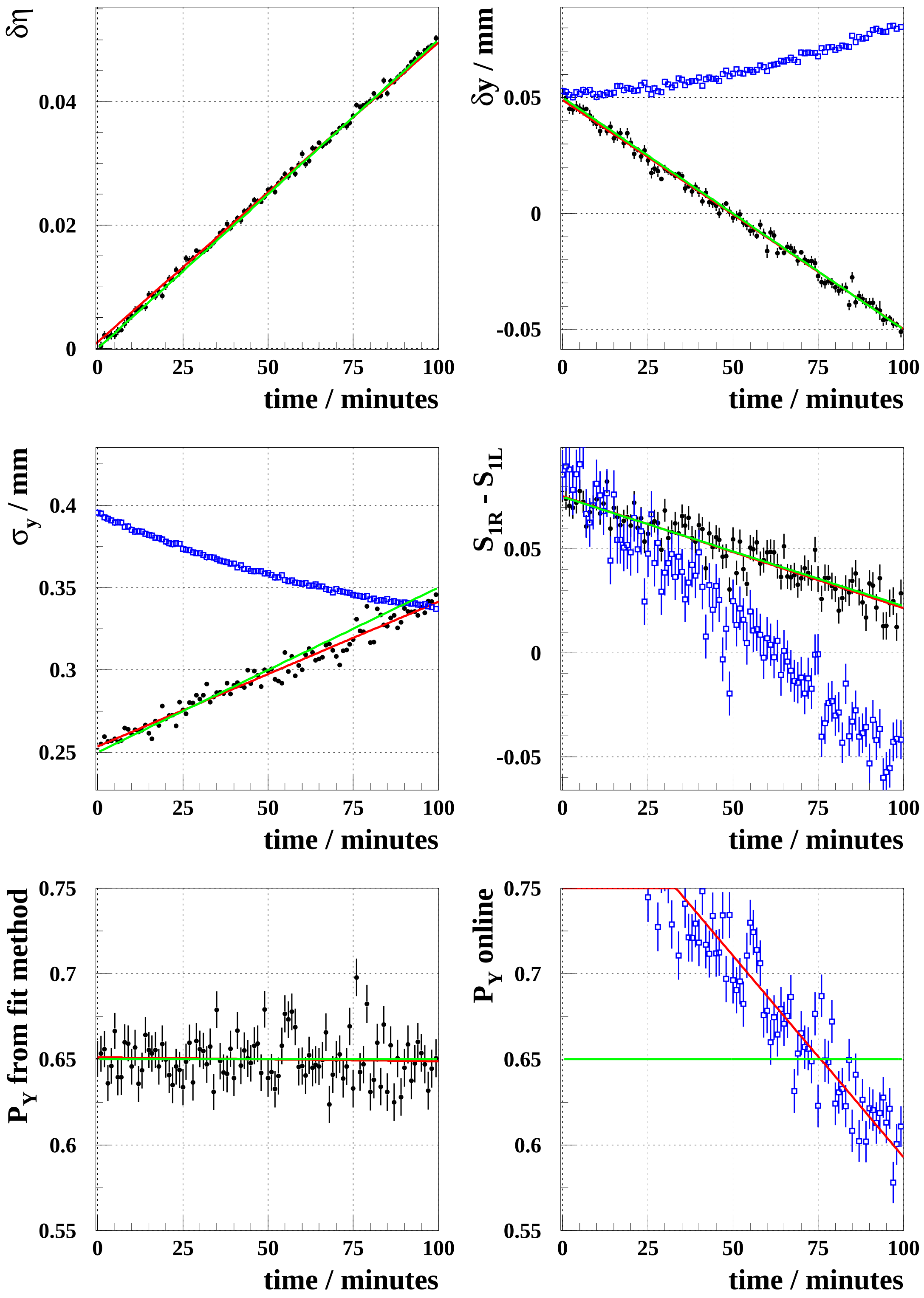

Figure 22: Systematic studies on MC simulations varying the five η–y–transformation parameters, the beam spot size, the vertical offset, the relative miscalibration of the calorimeter's up and down channels and the linear polarisation components of both laser helicity states: The green line shows the input values of the simulation, while the red line is a fit to the results of the reconstructed values from the new analysis, which are shown as black dots. The result of new analysis for the beam polarisation P_{Y} agrees well with the simulated values. The open blue squares show the results of the online analysis for comparison. For more details see text.